NUMERICAL INVESTIGATION OF THE RADIANT HEATING PERFORMANCE OF A CONTINUOUS ANNEALING FURNACE

A Thesis by

by

Gönenç Can Altun

Submitted to the
Graduate School of Sciences and Engineering
In Partial Fulfillment of the Requirements for
the Degree of

Master of Science

in the
Department of Mechanical Engineering

Özyeğin University
June 2021

Approved by:

Asst. Prof. Altuğ Melik Başol,
Department of Mechanical Engineering
Özyeğin University

Prof. Dr. Pınar M. Mengüç,
Center for Energy, Environment and Economy
Department of Mechanical Engineering
Özyeğin University

Prof. Dr. Tuba Okutucu Özyurt,
Energy Institute,
Department of Renewable Energy
İstanbul Technical University

Date Approved: 10 June 2021

To beauty and sublime

ABSTRACT

Annealing as a type of heat treatment process is widely used in the glass manufacturing industry. It is the last stage of the manufacturing process and has a highly dominant effect on the quality of the glass. Especially in large volume glass manufacturing the annealing process is carried out in a continuous type annealing furnace. In that furnace, the different stages of the annealing process are accomplished in the different zones of the same furnace. The main purpose of the heating zone of the furnace is to increase the temperature of the glass back to the annealing temperature. Due to the temperature levels reaching 923 K inside the furnace, radiation heat transfer has a dominant effect in this zone of the furnace. Due to the mostly nonparticipating nature of the furnace atmosphere, the radiation heat transfer is governed by the view factors between the glass and the furnace walls. At the wavelength range of the radiation emitted from the furnace walls, the glass can be modelled as opaque. Since the view factor between the glass and the furnace walls depend on the distance between the glass rows inside the furnace, the layout of the glassware could have a considerable effect on the heating effectiveness of the furnace. In this numerical study, a combined conduction–radiation solver was developed to investigate the heating characteristics of moving bottles inside the radiant heating section of a continuous annealing furnace. The solver was designed as a hybrid solver running the conduction and the radiation calculations on the CPU and the GPU (graphic processing unit) respectively. The radiation transfer between the opaque surfaces has been calculated with the Backward Monte Carlo Ray Tracing method. Running the method on the GPU, the computational cost of the radiation model has been massively reduced. Overall, 91% of the total computational time is spent by the radiation calculations and only 9% was taken by the heat conduction calculations. Moreover, two numerical methods regarding the integration of the radiation model with the heat conduction solver were developed. It was found that for the same level of accuracy the 2nd order accurate method enables to increase the time step in the transient calculations by a factor of 2.5 times concerning the 1st order accurate implementation. The considered furnace model consists of 29 bottle rows along the length of the furnace and with 15 bottles in each row. The initial temperature of the bottles was taken considering the moulding stage of the manufacturing line. The computational cost of the problem was reduced by considering the 7 rows of bottles in the computational domain. The developed algorithm enables simulation of the heat transfer across all the bottle rows using only a fraction of the entire row inside the furnace. Finally, a parametric study on the effect of the spacings between the bottle rows has been conducted. In this regard, the spacing between the bottles rows and the conveyor speed have been altered in a way that the throughput of the furnace, the number of bottles processes per unit time, is kept constant. The study shows that there is an optimum value for the spacing between the bottle rows. For the considered bottle form, this optimum row spacing value is found to be 35% of the bottle diameter.

ÖZETÇE

Tavlama bir tür ısıl işlem methodu olarak cam imalatı endüstrisinde yaygın olarak kullanılmaktadır. Üretim sürecinin son aşamasında tatbik edilir ve cam kalitesinde hâkim bir etki sahibidir. Yüklü sayıda cam üretimi gerçekleştilen ısıl işlem dizisi, özellikle sürekli tip tavlama fırınında gerçekleşir. Fırın içerisinde tavlama işleminin farklı aşamaları yine aynı fırının farklı bölümlerinde gerçekleşir. Fırının ısıtma bölgesindeki temel amaç; camın ısıtılarak tavlama sıcaklığına geri getirilmesidir. Fırın içerisindeki sıcaklığın 923 K mertebelerine ulaşması sebebiyle ışınım ile ısı transferi hayli önem arz etmektedir. Işınım ile ısı transferi iştirak halinde olmayan fırın ortamı sebebiyle çoğunlukla cam ile fırın duvarları arasındaki görüş katsayısına bağlı olarak hüküm sürer. Fırın duvarlarından yayılan ışınımın dalga boyu aralığında cam opak olarak kabul edilebilir. Cam nesnelerin fırın içerisindeki yerleşim planı, cam ve fırın duvarları arasındaki görüş katsayısı birbirine olan mesafeye bağlı olması sebebiyle fırının ısıtma etkililiği üzerinde hatırı sayılır ölçüde etkisi olabilir. Bahsi geçen sayısal çalışmada iletim ve ışınımı konu alan bir dizi işlem yürütücüsü geliştirilmiş ve bunun vasıtasıyla sürekli tip tavlama fırınının ışınımla ısınma bölümünde sürekli hareket halinde bulunan şişelerin ısınma niteliği ortaya koyulmuştur. Dizi işlem yürütücüsünde bilgisayarın merkezi işlemci birimi ve grafik işleme biriminden faydalanması nedeniyle

karma bir nitelik söz konusudur. Opak yüzeyler arasındaki ışınımla ısı transferi "Backward Monte Carlo Ray Tracing" adı verilen metot ile hesaplandı. Bu metot, grafik işleme birimini ile yazılımsam entegrasyonda bulunarak bilgisayımsal değerini büyük ölçüde azaltmıştır. Toplam bilgisayımsal sürenin %91 (yüzde doksan bir) kadarı ışınım ile ısı transferi işlemleri ve yalnızca %9 (yüzde dokuz) kadarı iletim ile ısı transfer işlemleri için harcanmıştır. Dahası ışınım modeline ilişkin olarak iki sayısal methot geliştirildi. Her iki metot için de aynı hassaslık değerinin yakalandığı aralıkta ikinci dereceden doğruluk sahibi metot, birinci dereceden doğruluk sahibi metoda nispeten birim zaman aralığını 2,5 (2 tam, onda beş) kat artırmaya imkan vermiştir. Gerçeklenmiş fırın modeli, her bir sırada 15 şişe olmak üzere toplamda 29 şişe sırasına elverişlidir. Şişelerin ilk, başlangıç sıcaklığı üretim hattının bir diğer bölümü olan kalıpma işlemi dikkate alınarak atanmıştır. Problemin bilgisayımsal değeri gerçeklenmiş fırın modeli içerisinde yalnızca 7 şişe sırası dikkate alınarak azaltılmıştır. Geliştirilen dizi işlem yürütücü, algoritma, fırın içerisinde bulunan 29 şişe sırasındaki her bir bardağın ısı transfer mekanizmasını sadece 7 şişe sırası dikkate alınması suretiyle bilgisayar tabanlı benzetimi mümkün kılmıştır. Şişe sıraları arasındaki mesafenin etkisi üzerine değişken eksenli ölçülendirme çalışması nihayet yürütüldü. Bu bağlamda şişeler arasındaki mesafeler ve taşıyıcı kayış hızı birim zamanda çıkan iş oranını sabit kılacak şekilde birbirine uyarlandı. Çalışma bulguları şişe sıraları arası mesafenin uygun bir değeri olduğunu ortaya koyuyor. Çalışmada kullanılan şişe şekline mukabil sıra aralığının uygun değeri, şişe çapının yüzde 35'i olarak bulundu.

ACKNOWLEDGMENTS

I would like to thank my family and relatives for their love, support and absolute discretion.
I would like to thank my childhood friends: Nihat Efe İşman, Ahmet Utku İşman, Tunahan Çakır, Yılmaz Berkay Demir, Fahri Ceyhan, Can Altun, Burak Çakıroğlu, Mete Kutay Kutlu, Berat Özbağ, Görkem Ülgen, Yusuf Kenan Bilhan, Kuthan Ulusoy, Kemal Canpolat, Batu Elkoca for the wonderful friendships and good memories we had. It is indisputable that some specialty who joined me during the years when my real preoccupations, a genuine and irresistable curiosity, which emerged in the secret of nature and full of joy with them, took over all my feelings and thoughts, and nothing could disturb.
I would like to thank Ömer Berk Yüksel and Gazihan Bakkalcıoğlu. They brought me another artistic perspective.
I would like to thank my friends from the office 502: Çağatay Emre Ayhan, Kaan Menekşedağ, Faizan Pervez Siddiqui, Athar Khodabakhsh, Gökçe Güven, Barış Büyüktaş, Berkay Halvaşi, Tolga Altınoluk, Ersin Yıldız, Kürşat Uzuner, Burcu Aygün.
I would like to thank my friends from the chemistry laboratory: Sinan Çoruk, Ezgi Gülçay, Ahsen Ünal, Ilgın Sandalcıoğlu, Alperen Burnaz and Kardelen Değermenci. Also, Dr. İlknur Eruçar for accepting me.

I would like to thanks Şerif Demirel, the security chef, for his clemency.

I would like to thank all member of Evateg. Ceren Cengiz and Alper Saygın have a great predence among them always. Great manners and composition have been taught to me by them. Head of the Evateg, Prof. Dr. Mehmet Arık, thanks to you for sharing experience, knowledge, guidance and compassion.

I would like to TÜBİTAK for the financial support during my research under the contract number of 117M420. Financial aid from Özyeğin University and utilization of computational resources was the foundation.

I would like to thank my advisor for accepting me. Working with him was such a joy and a bit challenging. He always pushed me further to do brand new things, always appreciated the idea and givve me complete encouragement during my research. He was like a brother and even a father figure, not only in the academic life, but also in the life. I would like to thank Prof. Dr. M. Pınar Mengüç for sharing his everlasting knowledge and deep understanding. In addition, the other member of the thesis defense committee, Prof. Dr. Tuba Okutucu Özyurt, I would like to thank for being a part of this journey and for her guidance and informative feedbacks.

I would like to thank to everyone who contributed to the production of uncontainable masterpieces: Dark Souls and Half-Life.

I would like to thank Dücane Cündioğlu. In the illuminance of his contemplation, I am struck by a great sense of lack. With passion, which is the greatest gift this gives rise to, I have clutched my artistry with a titan grip.

TABLE OF CONTENTS

LIST OF TABLES

LIST OF FIGURES

CHAPTER I

INTRODUCTION

Heat treatment is a combination of successive processes, is widely used in a variety of manufacturing industries such as plastic, metal, steel, iron and glass. They have a dominant effect on the mechanical and structural properties of the final products. Achieving such a high-quality product requires precise controlling of temperature within the material during processes. In that sense, heat treatment can also be defined as a compelled spatial distribution of temperature inside products in time trend.

Annealing as a type of heat treatment process is widely used in the glass manufacturing industry. The main purpose of annealing is eliminating internal stress development inside glass during solidification, as well as altering microstructures by cyclic operations without changing its shape. Annealing consists of heating, soaking and cooling operations that separately take place in three different stages of the same continuos furnace, consecutively. Firstly, glass is heated up to annealed temperature at the heating section, secondly, glass undergoes a soaking section of the furnace that involves keeping the glasses at an appropriate temperature until uniform temperature distribution is achieved within the glass, and finally, glass is carefully cooled down with adjusted rate in the cooling section involves slow cooling and rapid cooling. Processes are mainly dependent on five variables are temperature characteristic of the material, heating rate in the heating section, holding time in soaking section, cooling rate of cooling section and furnace atmosphere of each stage. Since the dependencies are highly associated with the heat, the heat transfer mechanism of the furnace must be clarified. All three modes of heat transfer mechanism are conduction, convection and radiation, actualize inside the furnace. Radiative heat transfer heavily depends set temperature of each zone in the furnace. In each zone, the main radiation source is the hot furnace walls. The hot furnace walls emit heat in the form of infrared light which is absorbed by the outer surfaces of the glass. Glass is transparent to the visible light, whereas infrared radiative energy incident upon glass surfaces can not penetrate through the glass that makes glass opaque. Heat can only dissipate by conduction inside opaque materials that leads temperature distribution is continuous from boundaries to the inner side [1], but especially in materials with low thermal conductivity such as in a glass, this leads to a high-temperature difference between the surface region and mid-region of the glass. To achieve a good quality product narrow range of temperature differences in the regions of glass is a must. However, temperature differences and corresponding internal stress can not be captured by the naked eye. In this regard, it is essential to precisely monitor the temperature of the glasses during the process. Nonetheless, the actual temperatures of the products inside the furnace can not be resolved due to technical limitations.

The temperature of each stage in the furnace has to be ceaselessly measured by thermocouples that installed during construction of the furnace. Because of the large dimensions of a furnace, achieving high temperature resolution in a furnace requires evenly distributing a large number of thermocouples. The temperature data of furnace received through thermocouples are monitored by PID controllers, which ensure that the zone environment is kept within a certain temperature range. The high temperature and chaotic combustion events in the region and the protective coating layer on the thermocouples adversely affect the accuracy of the measurement and often give erroneous data. Also, the measured data does not indicate the temperature of the glass to be treated, which is rarely in the thermal equilibrium with the furnace environment. In this context, there could be large temperature nonuniformities within the glass. Another thing is that the temperature of the glass is generally measured by the use of a pyrometer at the exit of the furnace. The drawback of pyrometer measurements is the resolution of time-dependent annealing process is completely shrunk and glass-furnace interactions during processes remain unknown. In this regard, numerical techniques can provide the temperature distribution of the glass during processes at the required resolution, and can give detail about optimizing furnace conditions for better treatment. However, their computational cost could be a limiting factor, especially in large scale industrial furnaces.

Industrial continuous annealing furnaces are generally longer than 20 m, wider and higher than 2m. Physically, multiple different stages, crowds of the product that can be more than 1,000 products to be processed simultaneously, complex geometries such as burners and glassware. In terms of physics, the three modes of heat transfer, combustion phenomena, interaction of fluids with moving solid product, temperature-dependent thermal properties such as thermal conductivity and specific heat capacity can be examples to be associated with the description of the annealing furnace. Computational power may not provide sufficiency to elaboratively represent the physical entity and the furnace of physics in detail. For that reason, a numerical investigation on annealing furnaces requires high fidelity models that minimize the cost of computational power requirements, provide numerical stability and capture differentiable and continuous entities of the annealing furnace. Moreover, annealing can be a time-consuming process that depending on which material is to be annealed. This time dependency can rapidly increase the total computational time of the numerical investigations. By virtue of that, GPU accelerated computing can be a good candidate to tackle computational time and accuracy of the simulations. GPUs are specifically designed to effectively perform rendering applications. They consist of many computing units that run in parallel and minimize the computational cost of the processing task..With the significant increase in computational resources and highly optimized algorithms in code libraries GPUs, it has become more popular among scientific research fields involving radiative heat transfer problems. A chief challanges in the radiative heat tranfer calculations are: the emission of the photons is spontaneous in the resulting directions and the emission points are random, each photon has distinctive propagation direction and energy, as the rays traverse across the medium, absorption, emission and scattering events can occur that affect direction and energy of the rays. Those challanges can be surpassed by GPUs that already showed tremendous speed-up over a traditional CPUs [2-8].

In this study, the heating characteristics of glass bottles in the radiative heating process of a large-scale continuous annealing furnace has been numerically investigated. The problem inside the furnace declared as a transient conduction-radiation problem. Due to the dominance of the radiative heat transfer inside the furnace the convective heat transfer is omitted. The effect of spacing between the rows of glass bottles in the radiant heating section of the furnace on the effectiveness of the radiative heating of the furnace is presented with developed model.

The developed numerical model is composed of individually two mutual schemes for conduction and radiation. The first scheme is interested in the temperature trajectories via prediction of heat conduction equation inside moving bottles by implicit Finite Volume Method with OpenFOAM framework on the CPU. The second scheme is conceptualized radiative heat transfer on the surface of moving bottles via in-house developed Monte Carlo implementation on the GPU. Due to nonlinearity of the radiation calculations the second order accurate radiation moel is introduced. The second order accurate model is derived from particularly successive iterations of the first order accurate model and they are compared. Two complementary schemes approached bottles as row-based rather than considering computational domain as unity. Developed hybrid solver with compatible second-order radiation model demonstrates high capability with feasible computational time with acceptable accuracy.

CHAPTER II

LITERATURE SURVEY

Many researchers have investigated the prediction of temperature distribution of products inside reheating/heating furnaces as well as furnace conditions. Thereupon, parametric studies are performed that possibly lead to increase furnace efficiency/performance. In this regard, studies are categorized into six sub-paragraphs. The first three paragraphs covered three main approaches to predict product and furnace conditions, in addition to their peculiar results. In paragraph four, only parametric studies are given. Paragraph five have very brief information about inverse analysis. The last paragraph, six, is showed common traits of presented studies under sub-titles.

In the first approach, studies include solving governing equations of reactive flows in unsteady state[9-10] simulations and steady-state [11-13] simulations. Gu et al. [9] numerically simulated the slab heating process with a simplified method of regenerative reversing combustion inside the regenerative walking beam furnace. The simplified method presents all burners have the same geometry all in zones, yet only burners' ability differentiates according to the zone. Slab movement is neglected in a furnace, however, corresponding burners abilities are changed to represent the movement. Simulation results are in good agreement with measured temperatures obtained by thermocouples. They have found that the heating time of a slab can be reduced 37min with their charging temperature is increased. Han et al. [10] investigated slab heating characteristics in a walking beam type reheating furnace. Skid posts and skid beams are included in the radiation calculations since they have a blocking effect of radiation heat transfer from hot gas to slab, and radiative heat fluxes are treated as a source term into flow and energy governing equations. To perform periodically transient movement of a slab, User-Defined Function(UDF) program is written and linked FLUENT. Computations are completed in 140 h with a 3.12 GHz Pentium 5 PC. Prieler et al. [11] analyzed 3D transient heating of steel billets with gas-phase combustion in a walking hearth furnace. Billets movement is considered as keeping them at the same position for 100 s before being moved and after heat flux is updated. They used an iterative solution procedure in which firstly steady-state simulation is conducted including combustion and radiative calculations, secondly determined heat fluxes are stored, after they served as boundary condition within transient heat conduction equation to be solved. This process is repeated until convergence criteria are found. Results have shown that fuel consumption of furnace can be reduced by oxygen enrichment in a gas mixture, and it has an influence that increases the furnace process efficiency up to 4%. Simulations are performed by commercial software package Fluent V15.0 and taken 10 days to complete. Han et al. [12] made numerical simulations of reheating furnace to estimate optimal residence time of slab. Slab movement is neglected in a furnace, only temperature data of slab is transported from the current position to the next position. Heat losses caused by skid system and furnace wall are included in the study and their contribution to the heat loss found as %12 and %3 of input heat respectively. They have found, furnace efficiency is kept decreased while residence time is increased, on the other hand, if residence time is short, a requirement of slab quality maybe not satisfied. The optimum time is found among five different residence time that is prescribed to be performed. Casal et al. [13] presented a new methodology for 3D simulation of steel billets inside walking beam type furnace. The movement of billets is considered as an additional source term into the general equation of energy transport equation in the solid region of billets while the transport equation remains the same for other solid regions in a furnace. In this way, the computational time is significantly reduced while keeping accuracy. Simulation results are validated with measurements. Power absorption of billets predicted with 0.5% of difference against real data, the overall model difference is indicated as 2%. The model is highly applicable to predict the possible changes that lead to better performance. *In the second approach*, studies have done by considering radiative heat transfer inside a furnace with transient heat conduction inside products [14-18] without flow modelling. Han et al. [14] tested appropriate residence time for the heating of moving slabs. Developed radiation code is parallelized by MPI library, to be able to overcome memory deficiency and saving computational time. Total computational time of the simulation is equal to residence time of slabs which is around 2h on a 16 clustered PCs (3 GHz CPU). Kim [15] developed a 2D mathematical model to predict heat flux on the slab and temperature within. Slab movement is defined as slabs are periodically moved on the next beam by the walking beam through the furnace. Results have shown that temperature increase is observed while slab emissivity and the absorption coefficient is increased, which is highly expected, but the final temperature near the exit is in narrow limits. Also, the presented model is in reasonable agreement with measured temperatures. Computations are done by 1.7 MHz personal computer in 1260 s. Emadi et al. [16] investigated heating characteristic of 3D billet by developed mathematical model. Zone method is used for radiation calculations. To calculate convective heat transfer coefficient at any location inside the furnace empirical correlation is used. An emissivity of wall in a certain temperature range is imposed constant, and wall and billet emissivity is independent of temperature that to be assumed. Assumptions are being made on the model that significantly reduced computational time without much accuracy lost. Iterative fashion is used to calculate temperature inside billets. Firstly, radiative and convective heat fluxes are determined by using a pre-given temperature of billet, wall and furnace gases, secondly, temperature inside billet is predicted by solving 3D heat conduction equation, finally, temperature variance is calculated between consecutive time steps. This procedure repeated until meet the constraint about variance and temperature difference. Effect of furnace wall emissivity is investigated since found that half of absorbed radiative heat flux on the surface of billets has been emitted from furnace wall. Augmentation in furnace wall emissivity does not have a significant effect on the final temperature of billet, however, it risen billet temperature on the non-firing and pre-heating zone of the temperature. Clearly stated that rising wall emissivity from its normal value 0.7 to 0.95 reduced billet residence time up to 5%. Jang et al. [17] have investigated a similar scenario of [16] but in 2D with including the effect of skids on the slab heating where the slabs are supported by fixed skids, and convective heat transfer coefficient is selected constant. It is observed skids are depressed the temperature of billets at the contact area. He also showed similar results with [15] about the effect of slab emissivity on the temperature profile of slab, and with [16] about the effect of wall emissivity on the temperature profile of slab. Harish and Dutta [18] computationally modelled heat transfer in direct-fired pusher type furnace within 2D steel billets. Convective heat transfer coefficient empirically determined. The effect of billets dimensions on the heating characteristic of billets is investigated. It is shown that surface and centre temperature of billets are decreased while billet thickness is increased, but does not considerably change final temperature. The residence time of billets according to a varied speed of billet is investigated where the dimension of billet remains the same. In the lower billet speed, 0.001 m/s, the temperature is rapidly increased at the early stages of the furnace but the corresponding residence time is 18 000s. The emissivity of billets is studied and found in the same relation with [15].

In third approach, studies have done by simplified but sophisticated reduced models. Dou et al. [19] numerically investigated the digital twin model of the annealing process of 3D coil cores with different sizes, positions and orientations. Three modes of heat transfer are valid. Heat conduction equation is solved by implicit finite volume method which is taken 5-7h. Convective heat transfer simulations with simplifications are performed by FLUENT that taken 20h. Radiative heat transfer calculations are done by thermal resistance network model, necessary view factors between surfaces are calculated by Monte Carlo based program that written in C# language and calculations taken 3-4h. Combined radiation and convection fluxes are served boundary conditions to the heat conduction equation. The digital twin model precisely predicts the temperature coil against experimental results. After validation, optimization has proceeded. The goals were reducing annealing time and keeping the quality of the material. For that purpose, the original annealing curve is implemented to the digital model as an initial condition. Next, an optimized annealing curve is operated inside a real furnace. With an optimized annealing curve, the required annealing time is decreased by more than 300 min and the measured quality of coil is approved by the standard. Optimization is also taken 5-7h. Depree et al. [20] developed a three-dimensional model for studying the temperature of steel strip in a continuous annealing furnace. The furnace has 160m and divided into 20 zones consist of 12 heating zone and 8 cooling zones. The cooling zone also split two zones inside itself. The 3D model involves complex geometries of furnace such: heart rolls, cooling tubes and steel strips with a couple of simplifications. The heat conduction equation is solved for the whole furnace including furnace walls. Convective heat loss of furnace surfaces is also taken into account. Radiative heat transfer calculations have covered all surfaces within the furnace and done by the hemicube method. The 3D model predicted temperatures are compared with measured furnace temperatures by thermocouples and good agreement was found. However, the 3D model demands high computational power and takes 9h for a fully scaled solution. To compensate for high demand, a 1D/2D reduced simple model is developed. Outcomes of the 3D model are used to improve simple models which can provide a highly rapid solution in around 10 seconds for a common desktop computer with high accuracy. Jadachowski et al. [21]. developed a mathematical model of simplified 1D quartz glass plates to investigate spatial-temporal temperature evolution during the heating process. 1D heat conduction equation solved by Finite Difference Method. Specific heat capacity and thermal conductivity considered temperature-dependent. Heat flow interaction involves thermal radiation between partially specular and partially diffuse gray surfaces, free convection and domain convection. Heat flow interaction added on heat conduction equation as a term. The view factor of the domain is solved by FE software ANSYS. The author indicated enclosure discretization in ANSYS leads to the numerical error that causes numerical errors in the calculation of view factors. Developed mathematical model verified by measured data and relative error of temperatures below 4.3%. Later, they extended their investigation with a 2D model on the same scenario [22]. In this model, forced convection is considered with the flow of inert gas through the furnace. Gas has a constant temperature and mass flow also considered transparent to radiation. Heat losses due to clamps are also added. Error is found as 4.4% against measurements. However, this model is found inappropriate for feedforward temperature control in the furnace in terms of its computational demand. Consequently, they derived a reduced-order finite element model that fit the new models [23]. After, the time average model is added to the model [24]. Results show that the uniformity of the specimen in a furnace can be improved by the oscillation of the specimen. Maislinger et al. [25] investigated essential non-linearities of horizontal direct-fired strip annealing furnace. For participants of the furnace which are flue gas, the rolls, the wall and the strip, used individual submodels. Each submodel covered all three modes of heat transfer. The model predicted temperature trajectories of strip, flue gas and the oxygen concentration in the chamber are very well matched with measurements. 1h furnace operation is simulated in 20min with standard desktop PC (IntelCorei5,2.5GHz,12GBRAM). The model is highly suitable for real-time control applications. Pytha et al. [26] developed a mathematical description of heating of a 1D plate in an annealing furnace by moving radiators are the only source. Net radiative heat fluxes onto the plate are consists of the heat flux emitted by the plate, the heat flux received from the moving radiator and the heat flux received from a reflective surface (shiny mirror) that reflects all radiation that came onto itself. The plate is assumed black body, so absorbs all radiation impinges on the surface of itself. All Emission and all reflection are considered diffuse. Radiative intensity obeys Lambert's cosine law. Convection does not take into account and radiation added to the heat conduction equation as a term. Model reduction is performed with Proper Orthogonal Decomposition is combined with Galerkin approach. To deal with an integral term in the model, one more ROM approximation is adjusted. The reduced model is compared with the full-scale model. The reduced model is accurately predicted the temperature within ±5K error bonds.

Also, several parametric studies have been conducted to reveal the possible enchancement leading to better furnace performance. Jacklic et al. [27] numerically examined the influence of the space between the 3D billets on the effect of productivity of continuous walking-beam furnace. Three different sizes of billets that are 180mm, 220mm, 300mm tested with the space between 0 to 250 mm with 50mm spacing. The longest reheating time is found for three sizes of billets on the condition where no spacing between billets. That is caused by the existence of a highly limited surface area of heat exchange between furnace and billets. When space between is billets are increased, furnace productivity is increased until space is reached its optimal point, where the maximum furnace productivity is achieved. Optimal spaces are respectively indicated as 80 mm, 100 mm, 120mm for different sizes of billets. Fatla et al. [28] suggested alternate gas circulation techniques inside the furnace. Unlike conventional circulation techniques, using a fan, they used rotating cylinders to generate gas circulation inside the furnace. Six different layouts of cylinders with different lengths and diameters, horizontally and vertically placed inside the furnace. Six different layouts are numerically simulated. It has been found that velocity is lower where the cylinder was horizontally placed (Layout 1,3,5) on the furnace bell than the cylinder vertically placed (Layout 2,4,6) on the furnace base. Furthermore, rotational flow induced by a rotating cylinder has a high influence on the distribution of temperature inside the furnace. Gas circulation provided more uniform heat distribution and improved gas mixing inside the furnace that leads to enhance thermal efficiency cycle of annealing. Han et al.[29] studied the thermal efficiency of reheating furnace. The entire furnace consists of fourteen sub-zones, and each zone is assumed to be a homogeneous temperature for both medium and wall. Medium and wall temperatures are calculated via heat balances. In each sub-zone, overall heat balances are taken into account as heat loss due to skid system, heat loss through the boundary of each sub-zone, thermal energy balance between inflow and outflow. The movement of the billets is taken into account as in [12]. Six different fuel feed conditions, CASE1-6, are tested. CASE4 was found as the most efficient that consumed the least fuel to obtain uniformity and high mean temperature. Also, it is shown that the proportion of fuel fed into the heating zones has no considerably effect in determining slab uniformity, the fuel feeding into soaking should be restricted, less than 20%, to get a good quality of slab. Han et al.[30] analyzed efficiency of Air-fuel and Oxy-fuel combustion in a furnace with a similar method in [29]. Aif-fuel mixture is heavily composed by 70% of and 21% of, on the other hand, Oxy-fuel mixture is 70% and 26% of, rest of the percentages belongs to other gases for both fuel each sub-zone. Five different cases are investigated, Air-fuel 1-2 and Oxy-fuel 1-3. Each case involves a different fuel feed rate. Results indicated fuel efficiency of Oxy-fuel cases are in the range of 71.1% - 74.2%, whereas Air-fuel cases are between 43.0% and 47.1%. under the operation condition of Oxy-fuel 1 and Air-fuel 2, predicted slab temperatures are almost the same. Based on computational results, Oxy-fuel 1 demonstrated 54% more fuel efficiency, overall. Garcia et al. [31] performed an analysis of the effect of heat recovery burners on the heating of billet inside walking-beam type furnace. Combustion is modelled with the Steady Diffusion Flamelet model defines a thermo-chemical component as a function of mean mixture fraction. The absorption coefficient of gases has no dependency on a wavelength. Four different burner conditions, S1-4, are tested. S1 belongs to the conventional burner and the other three belongs to self-recuperative. Results show that using self-recuperative reduced fuel consumption by up to 31%, increased production by up to 51% and overall average efficiency increased from 32.7% to 48%. While the furnace is enlarging, the contribution of radiative heat fluxes emitted from the furnace wall are decreased due to attenuation by flue gas absorption. On the other hand, the higher operating temperature of the furnace indicated less amount of absorbed heat flux by gases, resulting in more efficient heating.

Besides, since the dominant heat transfer mechanism in the domain is radiation emitted by the furnace, radiant boundary inverse problems can provide more insightful knowledge about the suitable configuration of heaters in the furnace, determining their appropriate number and their power to achieve desired thermal conditions on the products. Nevertheless, inverse problems have a notorious reputation for being ill-conditioned which means small changes in the problem tend to produce significantly large changes in the solution. It demands more attention in terms of numerical methods and computational time. 2D and 3D studies are given in References, respectively [32-35], [36-40].

General information about furnaces is conceptualized and briefly explained below, as the researches has very common approaches.

Heat transfer modelling

Transient heat conduction equation is solved to predict temperature distribution within products as 3D [11,13,16,19] and 2D [15,17, 22-24 and 1D [21,25-26]. As an essence of convection heat transfer calculations, convective heat transfer coefficient can be selected either constant value [17] or can be extracted from empirical correlation [16,21,25,31]. Radiative heat transfer can be calculated using finite volume method [14,15,17], discrete ordinates model [9-13], zone method [16], Monte Carlo [13,27] method or solving linear matrix [21-25]. Calculated radiative heat fluxes and convective heat fluxes can be served as boundary condition [9,11,14-17,27] or directly added as a source term [23-26,31]. For a radiatively active medium emitting, absorbing and scattering events [13,14,17,29] taken into account, or with non-scattering events [12,15,30]. For a radiatively inactive zones block-off method may be adopted [14,29].

Furnace Characteristics

Reheating and/or heating furnaces can have a large number of burners and extensive dimensions [10-17], and are generally divided into three zones, horizontally: preheating, heating and soaking [10-13,15]. Also, it might be split into multiple zones as well [9,14-15]. Medium temperature of sub-zones can be calculated by considering overall heat balances in each sub-zone, the temperature of furnace wall in each sub-zone can be directly calculated by applying boundary wall condition [30-31]. Another method is that they can be calculated from simulation [11] or they can be given as constant for each sub-zone [14-15,21-23,26]. Furnace boundary conditions are generally treated as diffusely emitting and reflecting [1-,12-15,21-23,30]. Furnace wall emissivity can be selected in the range of 0.7-0.8 [10-15]. Absorption coefficient of gas medium inside zones is obtained by WSGGM which is more accurate than the grey-gas model. [10-11,13-15,30-31]. For a modelling of turbulent combustion probability density function (pdf) along with fast chemistry approach [9-12], eddy dissipation model [13] and steady diffusion flamelet model [31] can be used. In the furnaces, a large portion of the radiative heat fluxes are occurred at the preheating and heating zones [9-11,14-16,31] due to the temperature difference is at the maximum between workpieces and furnace domain. The least portion of the radiative heat fluxes are occurred at the soaking zone [10,14,16], as we stated in the Introduction, soaking zone is only for achieving uniform temperature distribution within product rather than heating and cooling. Also, during heating process, the highest temperature gradients are developed at the edges and corners of the slabs [9-11,14-15]. Besides these, a large portion of convective heat fluxes have occurred at the early stages of the furnace but it is still relatively weak while comparing with radiative heat fluxes. Convective heat fluxes have a trend that their contribution to the heating is kept diminished through the furnace 10-11,13,16-17,31]. Main power consumption of furnace is occurred at the heating process by the products are absorbed heat, more than 40% of fuel energy. Second is heat dissipation as exhaust gases, more than 30%. The third is heat loss by skid system, more than 10%. Fourth is heat loss through a wall, just about 2%. Consumed energy for exhaust gases can be significantly recovered by warming up the combustion air however there is a tiny room for improvement of furnace efficiency by employing furnace wall insulation [12-13,29]. Fuel consumption of furnace can be reduced by oxygen enrichment in a gas mixture that leads to increase radiative heat transfer and combustion efficiency [11]. On the other hand, it is shown that the proportion of fuel fed into the heating zones has no considerably effect in determining slab uniformity, the fuel feeding into soaking should be restricted, less than 20%, to get a good quality of slab [29].

Product Characteristics

Complex movement characteris of the products suitably simplified to not contradict with CFD simulations do not tackle the movement concept of products by its default functions [9-16]. For example: Slab movement is neglected in furnace, only temperature datas of slab/billet is transported from current position of next position [12-14,29-30]. Properties of slab/billets are thermal conductivity, specific heat capacity can be selected temperature dependent [10-16,30], emissivity is 0.5 while $T < 1073K$ and 0.6 while $1073 < T < 1273$ [9,12,30] or it can be constant [31].

CHAPTER III

NUMERICAL METHODOLOGY

3.1 Annealing Furnace Model

Annealing process applied in the glassware manufacturing industry mainly consists of three stages that are heating, soaking and cooling stages. The different stages of the process take place in the different zones of the same continuous annealing furnace. The different zones of the continuous annealing furnace are depicted in the schematic that shown in Figure 1.

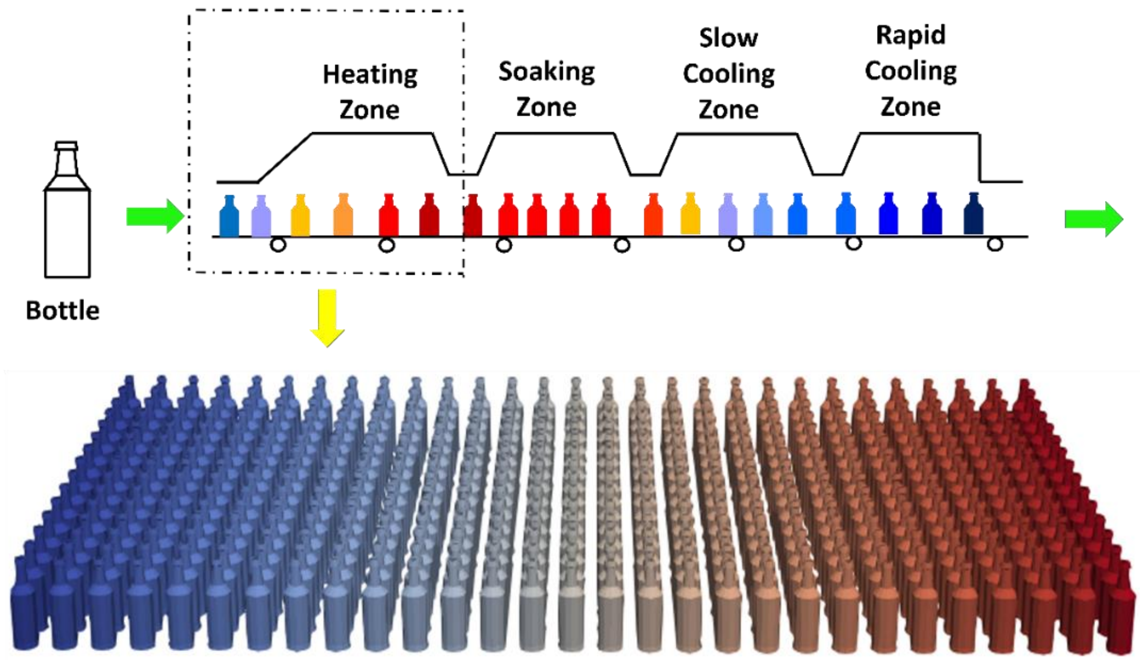

Figure 1: 2D demonstration of annealing furnace with closer looking 3D bottles inside heating section

In glassware manufacturing line the annealing process is the last stage of manufacturing. Hot glass coming out of the mold is directly guided into the annealing furnace. Meanwhile, the outer surface of the hot glass moving on the conveyor belt starts to rapidly cool down while it stays relatively hot on the inside. This nonuniform cooling behavior of the glass results in a nonuniform temperature distribution at the entrance of the annealing furnace. The main purpose of the heating section of the annealing furnace is to elevate the temperature of the glass back up to the annealing temperature. In this numerical study both the cooling process of the glass that takes place outside of the annealing furnace and as well as the radiative heating process inside the heating section of the annealing furnace were modeled. Accordingly, the temperature of the glass coming out of the mold is set to 1023K. Usually, a multitude of forming machines work on the same process line. In this study, 15 forming machines each delivering a new product every 10 seconds. Next, all the 15 glassware coming out of the forming stage are aligned and guided into the annealing furnace. They spend 90s on the belt until they reach the entrance of the furnace.

The heating section of the annealing furnace and the glassware to be annealed are shown in Figure 2. The furnace was designed a rectangular enclosure. The dimensions of the furnace and the layout of the bottles in the furnace and the dimensions of the glassware are given in Table 1. In total, 29 rows of bottles can fit inside the furnace and each row of glass consists of 15 bottles.

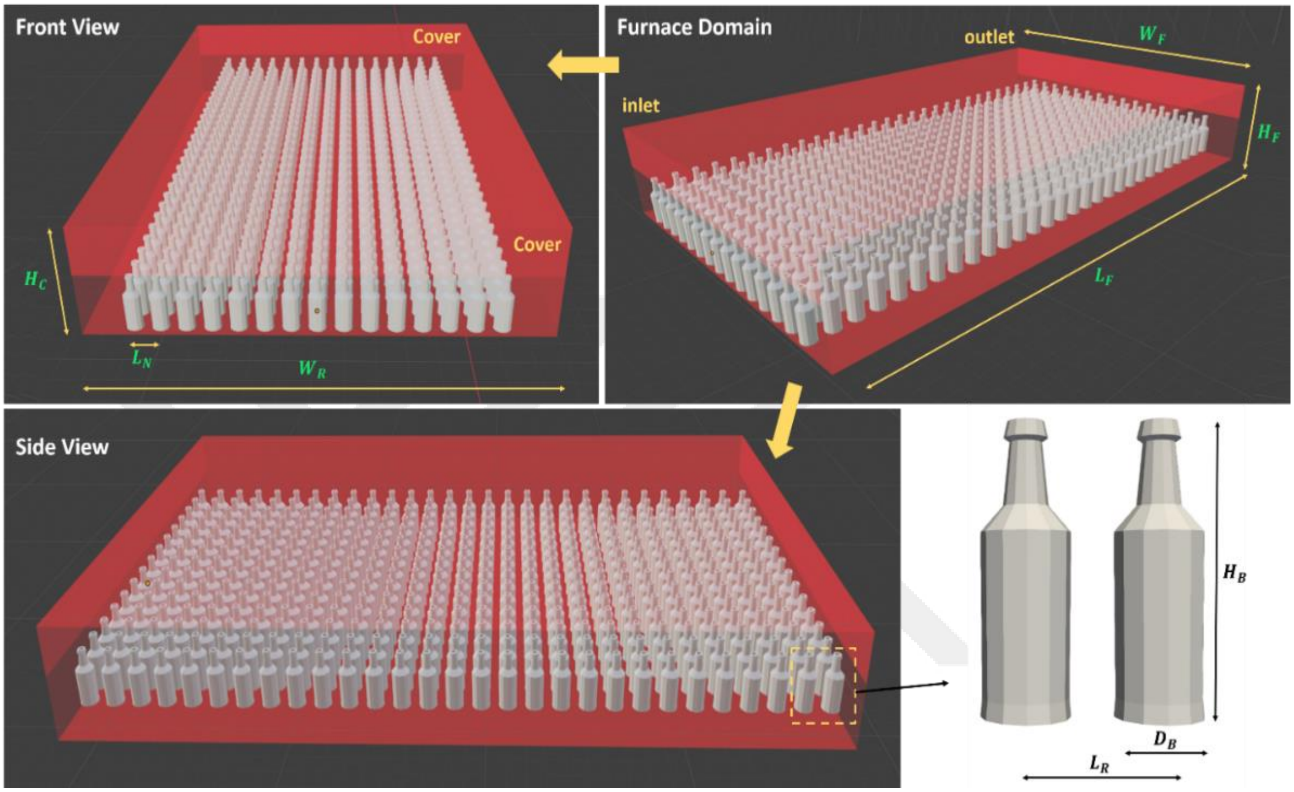

Figure 2: Heating section of the furnace within full of bottles

Table 1: Dimensions of the heating section

Length of furnace (L_F)	3.166± 0.685 m
Width of furnace(W_F)	2.160m
Height of furnace (H_F)	0.500m
Distance between rows (L_R)	0.1100 ± 0.0245 m
Distance between neighbor bottles(L_N)	0.120m
Width of bottle row (W_R)	1.762m
Height of the bottle (H_B)	0.245m
Diameter of the bottle (D_B)	0.0816m
Length of furnace cover(D_C)	0.30m

Heat transfer in the heating zone of electrically heated furnace is carried out with three heat transfer modes: conduction, convection and radiation. However, their contributions are quite comparable. Radiation heat transfer plays a dominant role. Approximately 75% of the furnace's heat transfer occurs through radiation in the first stage of the heating process. Convective heat transfer contributes to approximately 25% of the total heat transfer in the first phase of heating [41]. However, the contribution of convective heat transfer from the furnace inlet to the middle section continues to decrease. After this point, convective heat transfer does not play an important role in heating. Conduction takes place inside the bottles to dissipate the heat that has no role in heating, but the heat is transmitted from the conveyor belt to the bottles where the contact area is. However, it is a negligible small amount of heating compared to radiation and convection. In this study, the convective heat transfer effect and conduction effect from contact area are neglected due to explained reasons. The furnace atmosphere in electrically heated furnaces is nonparticipating and thereby the radiation transfer in the furnace occurs between the walls of the furnace and the glass. In this study, the temperature of the furnace walls was set to 923 K and they are considered as a black and diffuse emitter.

Glass is a semitransparent material. The transmissivity of the glass heavily depends on the wavelength of the radiation. As shown in Figure 3, the transmissivity of the 5 mm soda-lime glass heavily drops for wavelengths longer than 2.7μm. Only 20% of the energy of the incoming wave at 2.7μm can pass through the glass. And for wavelengths longer than 4.5 μm the transmissivity of 5 mm glass practically zero. In the same figure, the emissive power of a black body at 923 K is shown. Around 15% of the total energy is emitted by radiation with wavelengths smaller than 2.7 μm. The radiation emitted at wavelengths below 2.7 μm goes through the 5mm glass layer without being subject to a major absorption. 34% of the total radiation energy is emitted at wavelength between 2.7 and 4.5 μm. At this wavelength range, only 20% of the incoming radiation energy can pass through the 5mm soda-lime glass. So, treating the glass surface as black would lead to an overestimation in the incoming radiative flux by about 21%. Moreover, around 5% of the incoming radiation is reflected back due to the difference in the refractive index between air and glass. Considering all that, treating the glass as black results in around 25% overestimation in the incoming radiative heat flux. This is a considerable error. However, since the purpose of this thesis to investigate the effect of the layout of the glassware inside the furnace to the heating performance of the furnace rather than finding the temperature distribution of glass at the outlet of the furnace in an absolute sense, it is safe to assume that this modeling error would not considerably affect the results of this study.

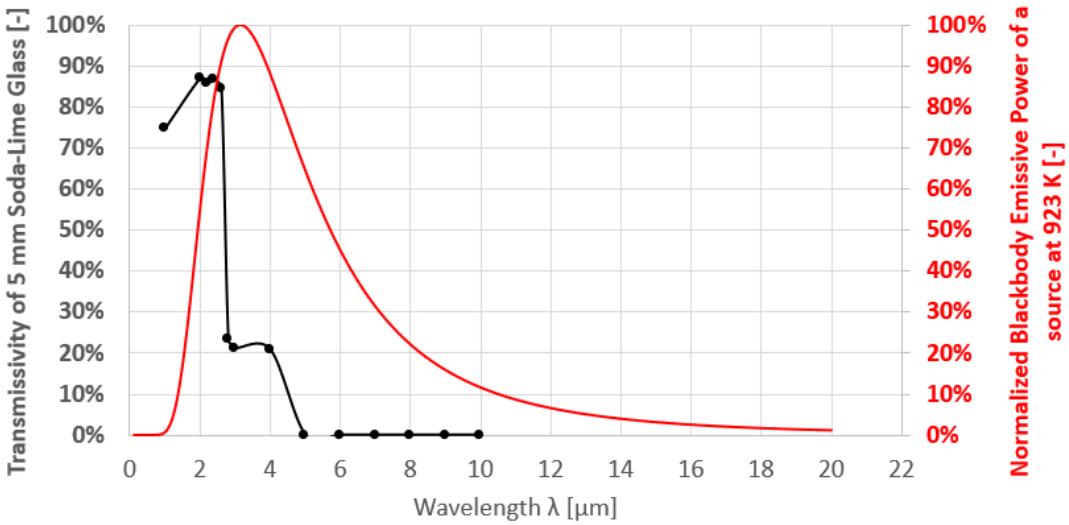

Figure 3: Emissive power of furnace walls and transmissivity of soda lime according to wavelength

3.2 Definition of the Optimization Problem

In the heating zone of the furnace, the view factor between the glass and the furnace walls have a considerable role in the heating process. In this regard, in a densely filled furnace the radiation incoming from the furnace walls will be blocked by the neighboring bottles. This shadowing effect negatively affects the heat transfer rate to the glass surface. However, one can increase the residence time of the glassware in a densely filled furnace and still have a high throughput from the furnace. On the other hand, a layout with the bottles being well separated would result in a high heat transfer rate to the glass but in this case the residence time of the glass must be kept very low to keep the throughput constant. These are the two extreme cases and the purpose of this study is to find the optimum spacing between the glass rows.

The objective of this optimization problem to find the optimum spacing L_N between the bottle rows that would minize the furnace length L_F.

$$\min \arg \ L_F(\, L_N)$$

The following constraints are also defined:

1. The minimum temperature of the glass must be equal or bigger than 850 K
2. The throughput of the furnace is set to 5400 bottles/h. In this regard, the speed of the conveyor belt is adjusted based on the spacing between the glass rows.

Other than these constraints, the initial and boundary conditions for the glass and furnace wall temperatures are shown in Table 2.

Table 2: Operation condition of the heating section

Initial condition of bottles	1023K
Temperature of furnace walls	923K
Conveyor speed	0.011 ± 0.002 m/s

3.3 Computational Domain

In this study only the heating zone of the furnace has been modelled. Even so, 435 bottles are present inside the furnace at any time. This number can slightly vary depending on the length of the zone and the spacing between the rows. Conducting a transient simulation with all 435 bottles is computationally highly costly. To reduce the computational cost of the problem the computational domain is restricted to 7 rows of bottles instead of the full 29 rows. Among 7 rows, the bottles in the very first row are not subject to any shadowing effect from the front side and thereby the bottles in that row heat up more quickly than the bottles in a real furnace. In a fully loaded furnace the shadowing effect is the same throughout the furnace. Due to the absence of the shadowing effect on the front side of the bottles, the temperature distribution of the bottles in the first row do not reflect the conditions inside the fully loaded furnace. The shadowing effect is present at the bottles in the 2nd row to a large extent as it is in a real furnace. However, the shadowing effect in the 2nd row is slightly lower than in the bottles in the 3rd row. In this computational model the bottles in the 4th row are representative of the actual conditions in a fully loaded furnace in terms of shadowing effect. However, the temperatures of the bottles in the other rows still need to be solved because they act as temperature boundary conditions for the bottles in the row 4. After all the 7 rows have been solved, only the results for the row 4 are stored for the temperature distribution of the bottles in that particular location of the furnace. In this way, all the rows of the furnace are solved. The schematic of the furnace model is showed in Figure 4.

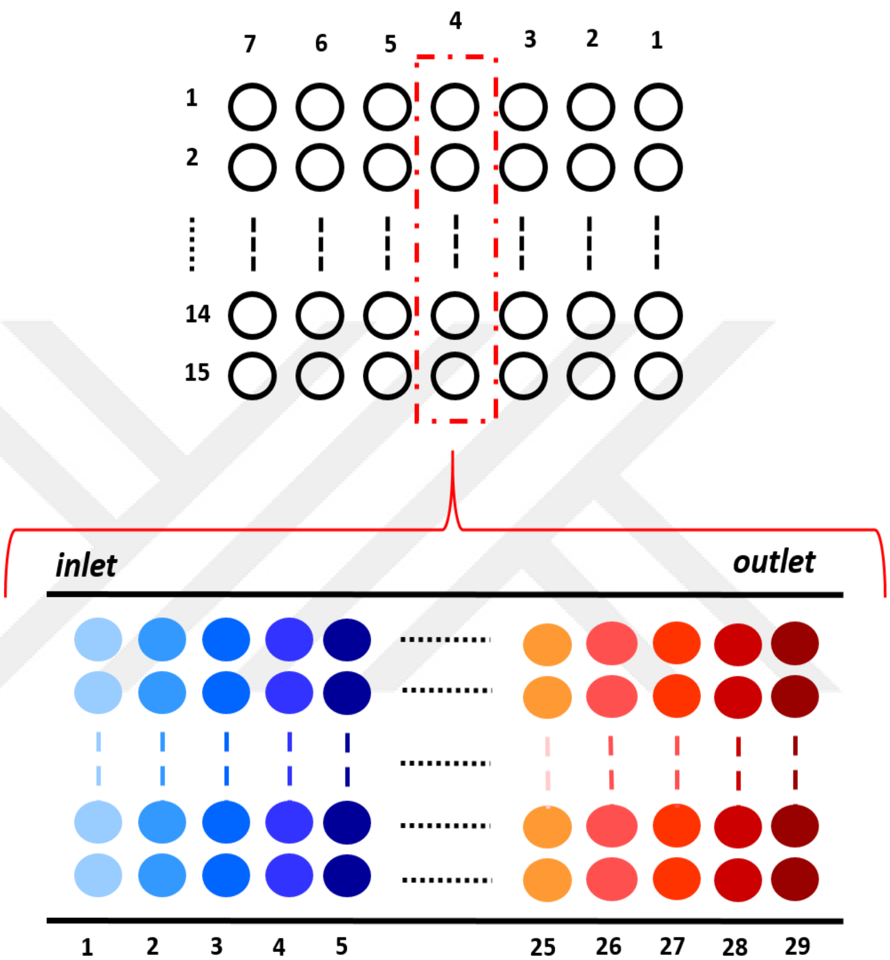

Figure 4: Computational model of the heating section

3.3.1 Bottle Mesh

The bottle mesh was generated in the commercial mesh generator Ansys IcemCFD that can be seen in Figure 5. A multi-block structured mesh topology was used. 10 cells have been used across the thickness of the glass. To preserve the uniformity of the mesh throughout the bottles in the same row, the same bottle mesh is used for all the bottles in the same row. The mesh statistics for a single bottle row mesh is given in Table 3. The generated mesh was finally converted into the OpenFOAM mesh file format. Apart from the volume mesh, the surface mesh of the bottles needs also to be extracted for the radiation model. Since the radiation model is compatible with only triangulated surface meshes, the quad type surface cells were triangulated by simply dividing each surface cell. Triangulation is being done by the association of diagonal vertices of each surface cell's face. That causes congruent triangles to rely on each cell face.

Table 3: Mesh statistics of the bottle row

Number of hexahedra cells	1,164,240
Number of surface meshes (primitives)	219,600
Max. aspect ratio	19.6892
Max. cell non-orthogonality	59.397°
Average cell non-orthogonality	18.413°
Max. skewness	1.64203

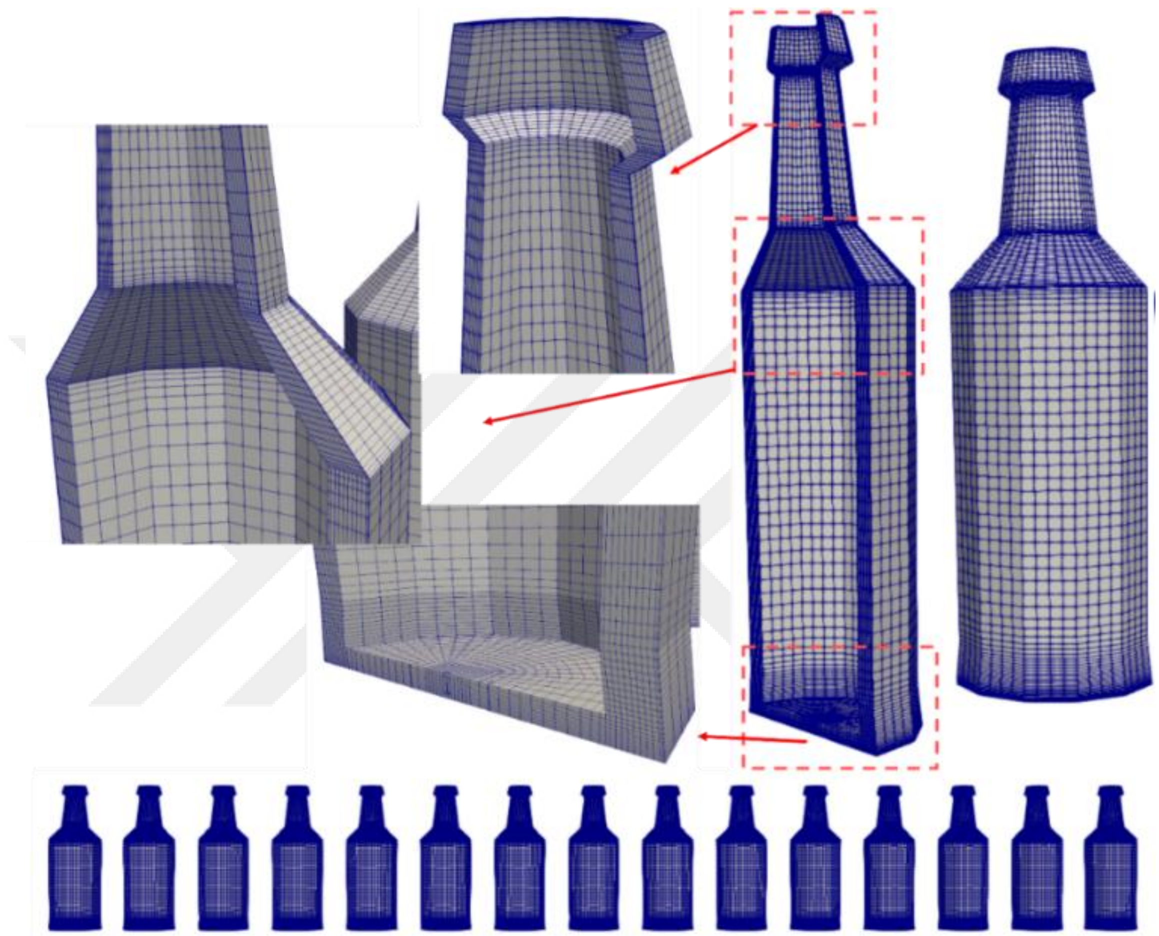

Figure 5: Solid mesh of the bottles that used in simulations

3.4 Combined conduction and radiation solver

A new solver for the combined conduction – radiation heat transfer problem was developed. The solver is designed as a hybrid solver where the conduction is solved on the CPU and the radiation model runs on the graphic processor (GPU). For the modeling of the heat conduction inside the bottle, the transient heat conduction solver *laplacianFoam* [42] solver in OpenFOAM repository is used. The solver uses a 2^{nd} order accurate central discretization scheme in space. For the time discretization the first order accurate Backward Euler method is used. In the same repository, the *fixedGradient* [43] boundary condition is selected for usage and was modified to accommodate for the incoming radiative heat flux on the glass surface during the runtime of simulations.

The radiative heat flux onto the glass surface is calculated with the inhouse developed surface-to-surface radiation model. Due to the nonlinearity of the radiative heat flux with respect to the surface temperature an explicit time discretization method is followed for the radiation model. Using an implicit time discretization for the radiation model would increase the computational cost of the solver considerably. The magnitude of the radiative heat flux depends on the 4^{th} power of the surface temperature difference. A slightly inaccuracy in the predicted temperature levels can result in a considerable error in the calculated heat flux level. To reduce the inaccuracy either the time steps have to be chosen sufficiently low which would increase the computational cost of the model or a higher order accurate method has to be followed numerically for the integration of the radiation model with the heat conduction solver.

Radiation heat transfer is occurred between the bottles in the same row, between the bottles in the other rows and between the bottles and furnace wall. In this study two different numerical methods have been developed regarding the temporal order of accuracy of the radiation model, explained below, and the flow chart of the methods is given in Figure 6.

3.4.1 The first order accurate model

Unlike the commercial solvers that treat the computational field as a whole, the developed algorithm divides the computational field into rowsets. In this study, the division is set to 7, as the computational domain consists of 7 rows of bottles. By that, the radiation and conduction calculations are performed row by row, rather than solving them at once. The calculation order of bottle rows is assigned sequentially from the first bottle row (1st row) to the last bottle row (7th row). Firstly, the surface temperature of all bottles and the furnace wall are mapped into the radiation solver. Secondly, the interior temperature of the first bottle is set into a conduction solver. Thirdly, the radiative heat fluxes that occurred on the surface of 1st bottle row is calculated concerning the surface temperatures of all participants in the domain at the time level t. By keeping the calculated radiative fluxes constant during the Δt time step, the transient heat conduction equation is solved and the temperature distribution in the time level $t + \Delta t$ is calculated. Right after new temperature field of the first bottle row is exclusively stored. When the first bottle row is solved, for the calculation of the second bottle row its interior temperature is assigned to the conduction solver. This procedure continued until all bottle rows are solved. Finally, once all bottle rows are solved their new surface temperature field is mapped onto the radiation solver and the all bottles are push forwward through the furnace. It's worthwhile to mention that the temperature field of all bottles individually stored and the radiative heat fluxes of the 3^{rd}, 4^{th} and 5^{th} bottle rows are particularly stored to the usage of further calculations which explained in the following title.

3.4.2 The second order accurate model

To improve the order of accuracy of the radiation boundary condition, the radiative heat flux calculations are repeated using the surface temperature distributions at the time level $t + \Delta t$. Having the radiative heat fluxes evaluated at two different time levels t and $t + \Delta t$, an average radiative heat flux value is calculated. Next, the average radiative heat flux distribution is used in the solution of transient heat conduction equation as a second order accurate radiative boundary condition. However, due to the additional cost of this higher order accurate method this approach is only applied to the 3rd, 4th and 5th bottle rows. The evaluation of the radiative heat fluxes in the remaining bottle rows is kept at the first order of accuracy. Since the thermal conditions in those bottle rows do not represent the conditions in a loaded furnace due to the lack of the shadowing effect, using a high order accurate method for those rows would be unnecessary.

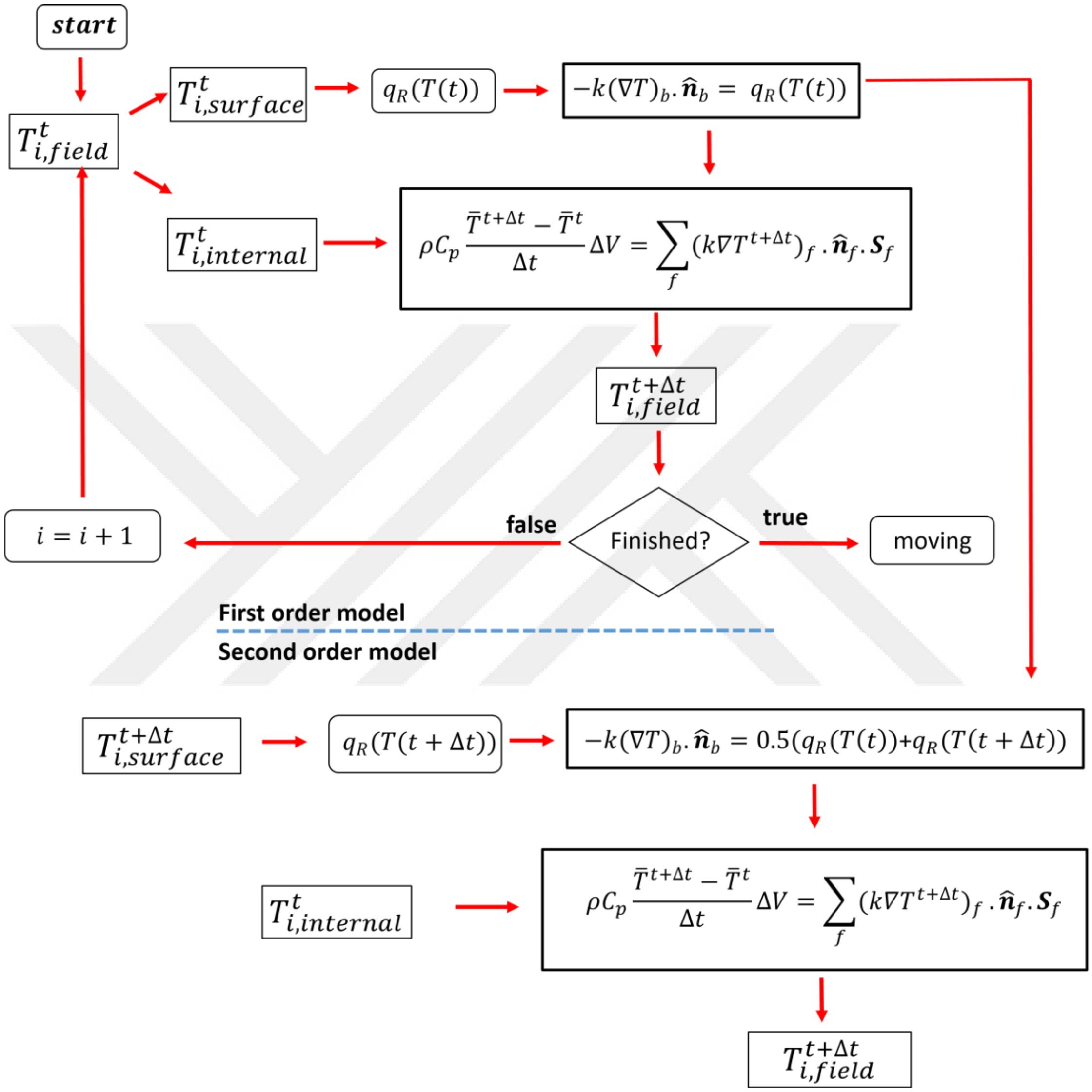

Figure 6: Flowchart of the hybrid solver

3.5 Surface-to-surface Radiation model

The surface to surface radiation model accounts radiative heat transfer between in an areas of diffuse surfaces without participating medium. Direction and carried energy of ray that emitted from surface area can not be changed while traversing to target area. In this condition, quantitative radiative heat transfer overly depends on deployment of the areas with respect to each other that can be accounted for by geometrical factor in given space referred as view factor. View factor proportions leaving amount of radiative energy from any given surface to that is incident upon target surface.

The view factor from source i to target j as differential areas that are shown in Figure 7 can be expressed as:

$$dF_{dA_i \to dA_j} = \frac{\cos(\theta_i)\cos(\theta_j)}{\pi s^2} dA_j \tag{1}$$

Since the real areas are taken into account, integral form of above equation over the surfaces i to j, then equation becomes

$$F_{A_i \to A_j} = \int_{A_i} \int_{A_j} \frac{cos(\theta_i)cos(\theta_j)}{\pi s^2} dA_j dA_i \tag{2}$$

Where s is the distance between the center of the finite areas, θ is the angle between centers with respect to each surface's normal, dA is the differential area of surfaces. This expression indicates that view factor is dependent on shape, orientation and distance. The reciprocity relation between finite areas can be written as:

$$A_i F_{ij} = A_j F_{ji} \tag{3}$$

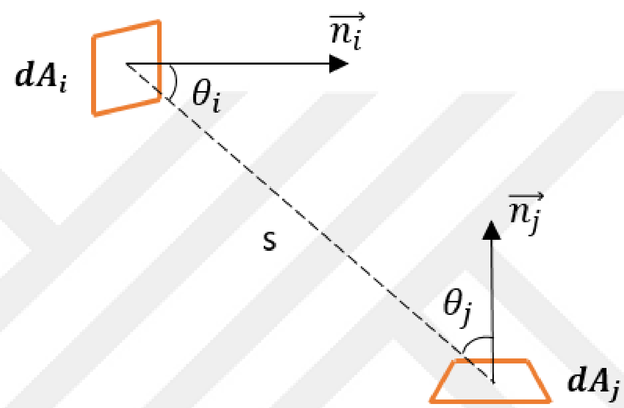

Figure 7: View factor between two differential areas

3.5.1 Radiation calculations between surfaces

The net radiative energy transfer between the surfaces is given by Equation 5.

$$\dot{\theta}_{A_i \to A_j} = \varepsilon \sigma F_{A_i \to A_j} (T_i^4 - T_j^4) A_i \tag{4}$$

Where ε is the emissivity of the surface, σ is the Stefan-Boltzmann constant, $F_{A_i \to A_j}$ is the view factor from i to j, T_i and T_j is the temperature of surface i and j respectively, A_i is the area of i and $\dot{\theta}_{A_i \to A_j}$ is the total amount of radiative energy strikes on area j that emitted from area i.

3.5.2 Backward Monte Carlo method

In-house surface-to-surface radiation model is developed by Backward Monte Carlo Ray Tracing method [44], so rays are being emitted from bottle surface instead of furnace plates. The ray emission points on the triangulated primitives (surface mesh) are calculated using uniform random sampling method. The coordinate of any point E_p on the primitives is expressed as

$$E_p = uA_i + vB_i + wC_i \tag{5}$$

where A_i,B_i,C_i are the coordinates of the vertices of the primitive *i* and u, v, w are the barycentric coordinates in the range [0 1] with u + v + w = 1

$$u = 1 - \sqrt{\xi_1} \qquad v = (1-u)\xi_2 \tag{6}$$

ξ_1, ξ_2 are random numbers between 0 and 1 and are generated using the Tiny Encryption Algorithm [27]. For a diffuse surface emitter, the polar angle θ and the azimuthal angle ψ of the rays are expressed as

$$\theta = \arccos(1-2\xi_3) \qquad \psi = 2\pi\xi_4 \tag{7}$$

where ξ_3, ξ_4 are uniform random numbers generated also by the Tiny Encryption algorithm. The rate of heat emitted from the surface element *i* is defined as

$$E_i^{emit} = \sigma T_i^4 A_i \tag{8}$$

where σ is the Stefan-Boltzmann constant, T_i is the temperature and A_i is the area of the primitive *i*. Rays emitted from the same primitive *i* all carry the same amount of energy $E_{ray,\, i}$

$$E_{ray,\,i} = \frac{E_i^{emit}}{\text{number of rays}} \tag{9}$$

After the rays are released, the radiative energy absorbed by the surface element j is calculated by adding the energies of all the rays hitting on the surface element j.

$$E_j^{absorb} = \sum_{i=1}^{n} \sum_{k=1}^{m} E_{ray,\,i,\,k} \tag{10}$$

where n is the number of total primitives and m is the number of rays hit on the primitive j emitted from the same primitive *i*. The same primitive j also emits radiation to the surrounding calculated in the following way.

$$E_j^{emit} = \sigma T_j^4 A_j \tag{11}$$

The net rate of incoming radiation heat transfer on the surface element j is expressed as

$$\dot{Q}_j = E_j^{absorb} - E_j^{emit} \tag{12}$$

Finally, the net radiative heat flux on the surface element j is calculated.

$$\dot{q}_j = \frac{\dot{Q}_j}{A_j} \tag{13}$$

Ray traversal is tracked for the purpose of radiative heat transfer exchange between objects in the domain. Net radiative heat fluxes are computed for each primitive by summation of energy that carried by rays are absorbed and emitted.

Radiation model implementation is carried out using the Optix Ray Tracing Engine [45] developed by Nvidia.Ray tracing calculations are computationally intensive. In the naïve implementation one has to consider the intersection of each ray with every primitive in the domain. However, the computational complexity of the method can be dramatically reduced by the use of advanced data structures called acceleration structures. In the current implementation Bounding Volume Hierarchy (BVH) of Axis Aligned Bounding Boxes (AABBs) [46] is selected as the acceleration structure of the geometrical model. In 3D space, the objects in the domain are enveloped by AABBs to accelerate the performance of ray traversal. AABBs must be as tight as possible to perform ray/triangle intersection more efficiently. After the rays are launched, first the intersection of the rays with the bounding boxes are checked and then the search for the particular primitive is carried out only for the primitives inside the bounding box.

3.5.3 Implementation Details in the Optix Library

In radiation model tasks are distributed among three programs that are emission program, hit program and calculation program.

3.5.3.1 Emission program

The emission program is the mechanism for the preperation, calculation and execution. In preperation, the number of rays to be emitted per face is calculated first. After, the direction and emission points of individual rays are determined. In calculation, the radiative energies to be imposed onto individual rays are calculated, and imposed. In execution, rays are launched from he each face.

3.5.3.2 Hit program

The hit program is called when emitted rays intersect any face in the computational domain. When the intersection is found, the amount of radiative energy carried by intersected face is absorbed according to its view factor to the face that are emitted intersected rays.

3.5.3.3 Calculation program

Calculation program determines net radiative heat fluxes per face by summing of released energy and absorbed energy. Calculations are performed by atomic operations.

3.6 Efficiency of Backward Monte Carlo Ray Tracing method

To prove the robustness of the in-house developed radiation model, the Backward MCRT method and Forward MCRT method are contrasted. In this regard, a very simple case is originated from the coaxially parallel squares with a different edge length in the 3D domain [47] and showed in Figure 8.

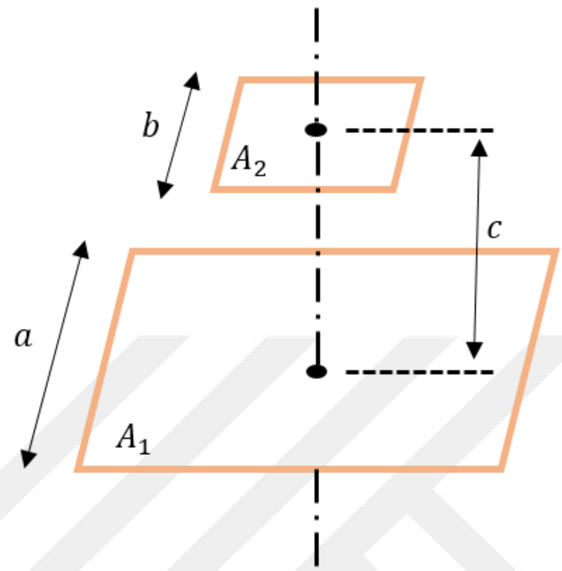

Figure 8: Simple validation model

The analytical solution of the case is derived by Crawford and Martin [48] and the solution is expressed in [49]. In this case, a is selected 10, b is 1 and c is 5. The numerical calculations are performed by two different cases:

1) Rays are being emitted from the large square A_1 and the corresponding view factor F_{12} is directly calculated. This is considered the Forward MCRT method.
2) Rays are being emitted from the small square A_2 , however the view factor F_{12} is calculated by Equation 4 with using F_{21}. This is considered the Backward MCRT method.

Emitted number of rays are selected as $32^2, 64^2, 128^2, 256^2, 512^2, 1024^2, 2048^2, 4096^2$.

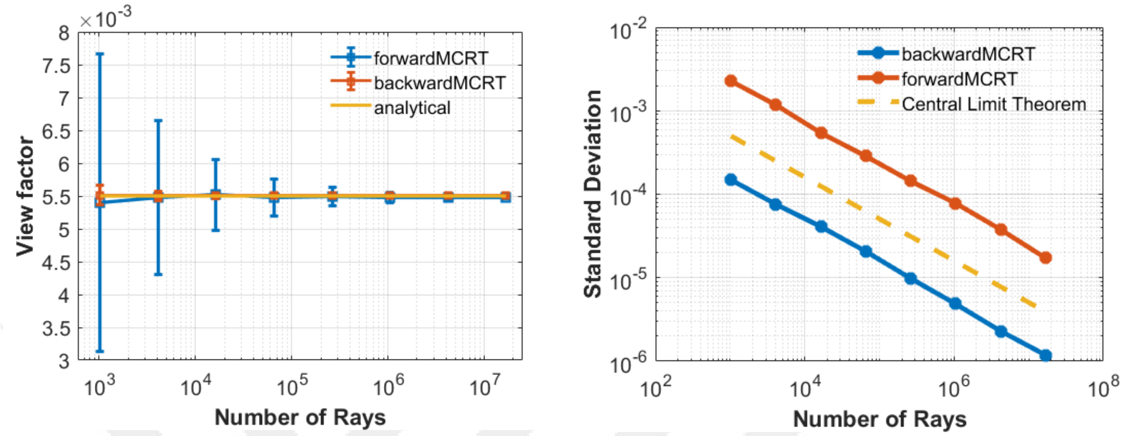

Figure 9: View factor according to number of rays and comparing corresponding standard deviation

Figure 9 shows the calculated view factor of F_{12} by Forward MCRT and Backward MCRT. The calculated view factors are the mean of 500 individually random simulations carried out with different numbers of rays. As shown, the higher number of rays being emitted, the closer is the calculated results to the analytical and, the standard deviation tend to decrease. The standard deviation of the Forward and Backward MCRT is compared in the below graphic. The decrease in standard deviation is in line with CLT. Moreover, the contrasting of two methods revealed that the same level of standard deviation can be achieved by Backward MCRT with nearly using 256x fewer rays which is indicated the efficiency of the method.

3.7 *Merits of Quantifications*

3.7.1 Accuracy test of radiation model

Monte Carlo is a statistical method that generates repeated random samples from the probability distribution, which is very useful to accurately estimate unknown distribution. Due to its statistical nature, the Monte Carlo method develops uncertainty that depends on the size of the random samples. However, this accompanies one advantage and one disadvantage. The disadvantage is that accuracy of the model is heavily depended on the size of the random set obtained by repetition of random sampling. So the higher number of samples in the data sets results in higher accuracy. High number of samples demands more computational power however. The advantage is that the method is independent of mesh properties as opposed to traditional mesh based methods such as the finite volume method, discrete coordinate metdo and zone method. The mesh only serves as a principal domain of the random sample generation event. The advantage becomes more when the geometries are getting more complex.

A measure of the uncertainity of the sample size is standard deviation that given as follows:

$$S_x = \sqrt{\frac{\sum_{i=1}^{n}(x_i - \bar{x})^2}{n-1}} \tag{14}$$

where n is the size of the data set, x_i is the indivual sample of the data set and $\bar{x}$ is the mean of data set. A lower standard deviation indicates that the samples in the data set become statistically significant. Thus, the contribution of individual samples becomes close to the mean of samples. In this study, x_i is the radiative heat fluxes on the surface of bottle row and $\bar{x}$ is the mean of heat fluxes. According to the Central Limit Theorem (CLT), the decrease in standard deviation is proportional to $1/\sqrt{N}$. Meaning that for a factor of 2 reductions in the standard deviation the number of rays used in the calculation must be increased by a factor of 4.

3.7.2 Likelihood test of models

Root Mean Square (RMS) is a common practice to quantify the similarities between models. RMS value can only be equal to or greater than 0 (zero). A value of 0 indicates a perfect match between models. However, in a very large data sets which governed by randomness such as Monte Carlo method, it is very hard to achieve. On the other hand, a value greater than 0 indicates dissimilarities between models. While compared models are differentiated from each other, the value becomes greater than 0. For achieving better model, the value should close as much as possible to the 0. The equation used for RMS calculations is given as below.

$$\Delta \mathrm{T}_{\mathrm{rms}} = \sqrt{\frac{1}{\mathrm{N}} \sum (\mathrm{T}_{\mathrm{ref}} - \mathrm{T}_{\mathrm{model}})^2} \tag{15}$$

where T_{ref} is the variable value of reference model, T_{model} is the variable value of model to be tested and N is the number of samples. In this study, T_{ref} belongs to reference surface temperature, T_{model} belongs to surface temperature of first order accurate model and second order accurate model and N is the number of faces on the surface of bottle row.

3.7.3 Volume average calculations of temperatures

Volume average calculation is the average of a values with the function variable is weighted by relational indicator. In this study, the function variable is computational cell-based temperature and the indicator is computational cell volume. The formula of temperature volume average calculations is given below.

$$T_{avg}^{i} = \frac{\sum_{j}^{N} T_{cell}^{i,j} V_{cell}^{i,j}}{V_{total}^{i}} \tag{16}$$

where i denotes bottle numbers, N is the number of computational cells, T_{avg}^{i} is volume average temperature of bottle, $T_{cell}^{i,j}$ is a temperature of computational cells, $V_{cell}^{i,j}$ is the volume of computational cell and V_{total}^{i} is the volume of digital bottle.

CHAPTER IV

RESULTS

4.1 Accuracy of the radiation model

Radiative heat fluxes imposed on the glass surfaces are calculated with the Backward Monte Carlo Ray Tracing method. Due to its statistical nature, a measure of the accuracy of the model is standard deviation that lies in surface radiative heat fluxes. The number of rays used in the heat flux calculations, set the standard deviation in the results. To evaluate the number of rays required for a given standard deviation level, calculations are repeated with an increasing number of rays and the resulting standard deviation levels are derived. In this regard, rays are released from the surface of the bottle at the center of the 4th row. 14, 355 and 910 rays per boundary element (primitive) are launched. Given results are mean of 1000 iterations performed independently. Figure 10 shows the mean radiative heat fluxes of 1000 independent calculations each carried out with the same number of rays per boundary element. The error bars represent the standard deviations in the calculated heat flux values. As clearly can be seen on the upper part of Figure 10, there is no significant changes in terms of mean value of the heat fluxes, however standard deviation of the heat fluxes reduces with the increase in the number of rays. The highest standard deviation is obtained when 14 rays are used per primitive. In this case the level of the standard deviation with respect to the mean heat flux value is around 20%. Using 355 rays per primitive results in a standard deviation that is about 3.5% of the mean heat flux level. The lowest standard deviation is obtained by 955 rays used per primitive which indicates about 2% of the mean heat flux level. Although there is an accuracy difference of about 1.5% between the 355 rays per primitive and 955 rays per primitive, it is not considered noteworthy to increase computational effort. Consequently, 355 rays are used per primitive in the furnace calculations.

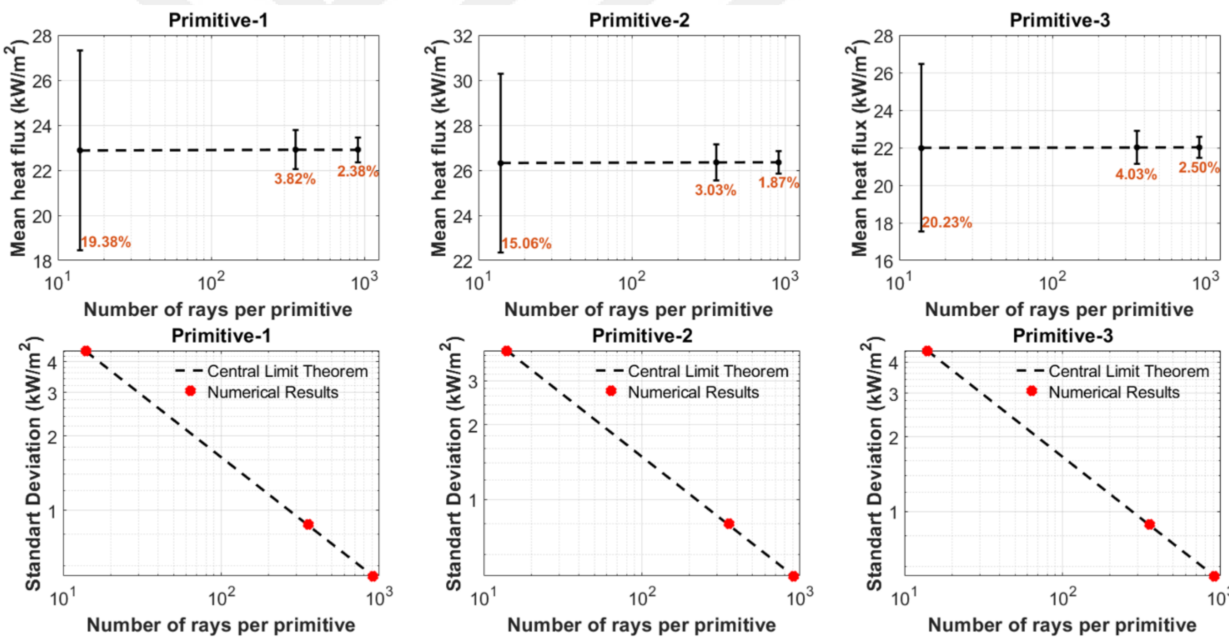

Figure 10: Mean of radiative heat fluxes and their standard deviation according to number of rays

4.2 Effect of Time Step on Accuracy of the models

To investigate the effect of the time step (Δt) on the accuracy of the calculations, the simulations are performed with 1s, 2s, 5s and 10s using both the first and second order accurate radiation models. Surface temperature distribution of bottle on the middle of 4th row is collected 30 seconds after the bottle row is entered the furnace. To exclude the effect of the random error due to the Monte Carlo calculations the radiation calculations were repeated with the same random number sequence for different evaluations of the radiative heat fluxes. This ensures that the effect of the random error is the same in all the calculations and the differences in errors are only due to the time discretization. Figure 11 shows the rms of the temperature difference between the calculations conducted using different time steps. Here, the reference solution is considered the solution of the first order accurate method that is used with a very low time step of Δt = 0.25s.

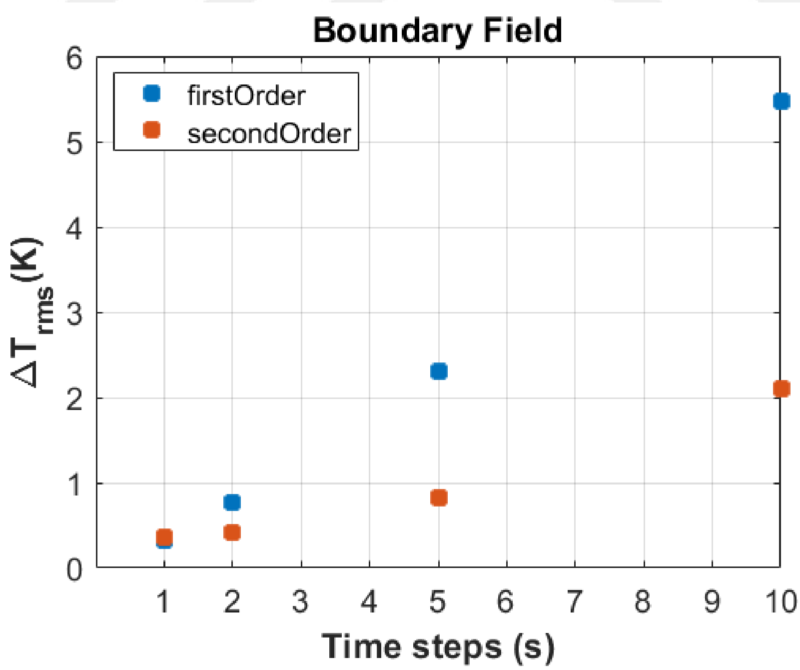

Figure 11: RMS of both first order accurate and second arder accurate radiation models according to time steps

As expected, deviation of both models is growing while time step value is increased. The error rate of both models is almost equal with Δt =1 s, which is less than 0.5 K. On the other hand, with Δt =2 s, the error rate of both models is started to differentiate and becomes comparable. The error rate of first order accurate models significantly increased to 0.9 K, but the error rate of second order accurate model still less than 0.5 K. With Δt =5 s , the error rate of first order accurate model exceeded 2 K, however error rate of other model is less than 1 K. In addition to that, the error rate of first order model with Δt =2 s and second order model with Δt =5 s has roughly same. With Δt =10 s, first order model's error more than 5 K yet second order model's error is around 2 K. Moreover, error rate of second order model with Δt =10 s is smaller than first order model's error Δt =5 s. In short, second order model's accuracy surpasses first order models while time step is increased. Considering all that, the second order accurate model with Δt=5 is found to be suitable in terms of the computational cost and accuracy for the furnace heat transfer study. It results in temperature errors less than 1 K.

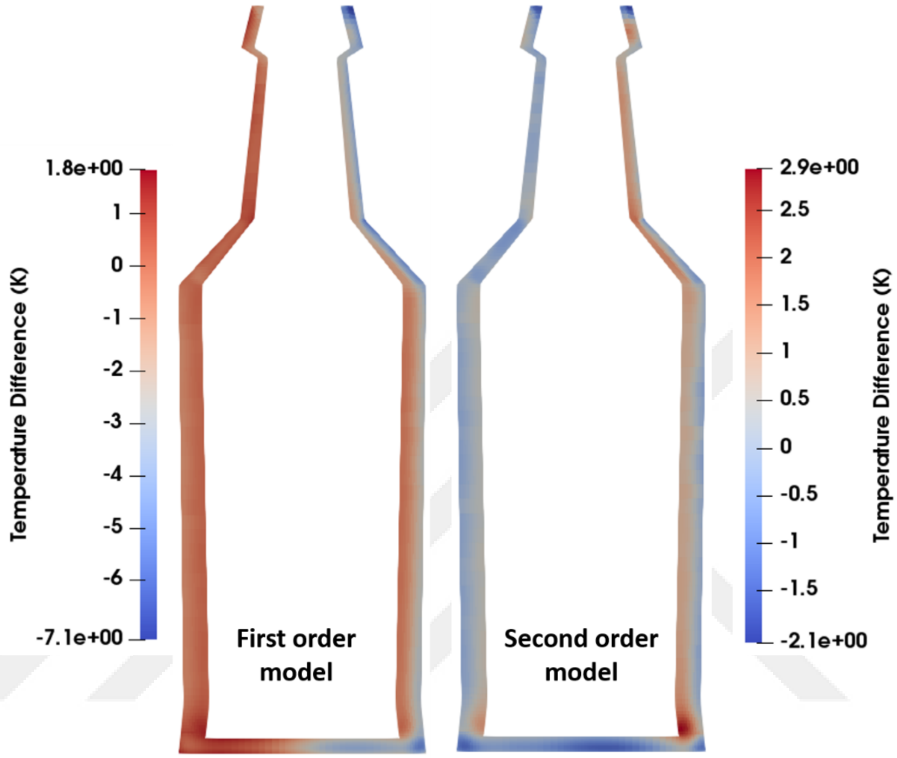

Figure 12: Temperature differences inside bottle for both first and second order radiation models.

Figure 12 shows the temperature error of the two methods with Δt = 5s with respect to the reference solution calculated with the first order accurate method and with Δt = 0.25s. For both models, highest temperature errors at the base, shoulder and mouth of the bottles. Respectively, for the first order model they are approximately 8K, 6K and 5K and for the second order model they are 3K, 2.5K and 3.5K. Temperature errors are greater laterally and vertically in first order accurate model compared to second order accurate model. Second order accurate model predicts more accurate and shows less biased results.

4.3 Validation of computational model

As mentioned before, a total of 7 bottle rows were included in the computational domain. The presence of the additional rows was to provide the required shadowing effect on the central row (row 4). Related with the shadowing effect is the view factor between the different bottle rows. Table 4 shows the view factor between the different bottles in the central row (4^{th} row) with the bottles in the other rows. Results show that around 35% of the view factor is between the bottles in the central row and the furnace walls. Around 50% of the view factor of a bottle is with itself. The remaining view factor is with the other row of bottles which is also drops with the spacing between the bottle rows. The edge bottles have the highest view factor to the furnace walls. View factor of 2^{nd} bottle to the furnace wall is decreased about 6%. After that point to the middle bottle, there is no significant change in the view factor. This trend has accordance with the temperature distribution inside furnace (Figure16) as well. First and last row have the least view factor to the 4^{th} row. More than 95% of the radiative heat exchanges are occurred among 3^{rd} row, 4^{th} row, 5^{th} row and furnace plates. That is the reason why second-order calculations are only performed for those three rows.

Table 4: View factor of 4th row to the other rows

Bottle Numbers	**Furnace Walls**	1^{st}& 7^{th} $Rows$	2^{nd}& 6^{th} $Rows$	3^{rd}& 5^{th} $Rows$	$4^{th}Row$
1 & 15	0.4143	0.0021	0.0063	0.0512	0.4661
2 & 14	0.3411	0.0035	0.0112	0.0678	0.4915
3 & 13	0.3311	0.0040	0.0120	0.0725	0.4917
4 & 12	0.3282	0.0040	0.0124	0.0734	0.4917
5 & 11	0.3274	0.0041	0.0125	0.0737	0.4917
6 & 10	0.3270	0.0042	0.0125	0.0739	0.4917
7 & 9	0.3268	0.0042	0.0125	0.0739	0.4917
8	0.3269	0.0042	0.0125	0.0739	0.4917

4.4 Parametric study of optimum row spacing

To assess the effect of the spacing between the rows on the radiative heating of the bottles, simulations with different spacings between the bottles were conducted. The spacings between the rows and the furnace length are calculated with the following equations

$$L_F = V_C * t_r \tag{17}$$

$$V_C = L_R / t_A \tag{18}$$

Where L_F indicates the length of furnace, V_C is the speed of conveyor belt, t_r is the residence time of bottles, L_R is the distance between rows, $t_A$is the deliviring time interval of bottle row by forming machines. Speed of conveyor belt is adjusted according to distance between rows in every scenario. That adaptation guarantees true furnace output, 5400 bottles in one hour, remains the same.

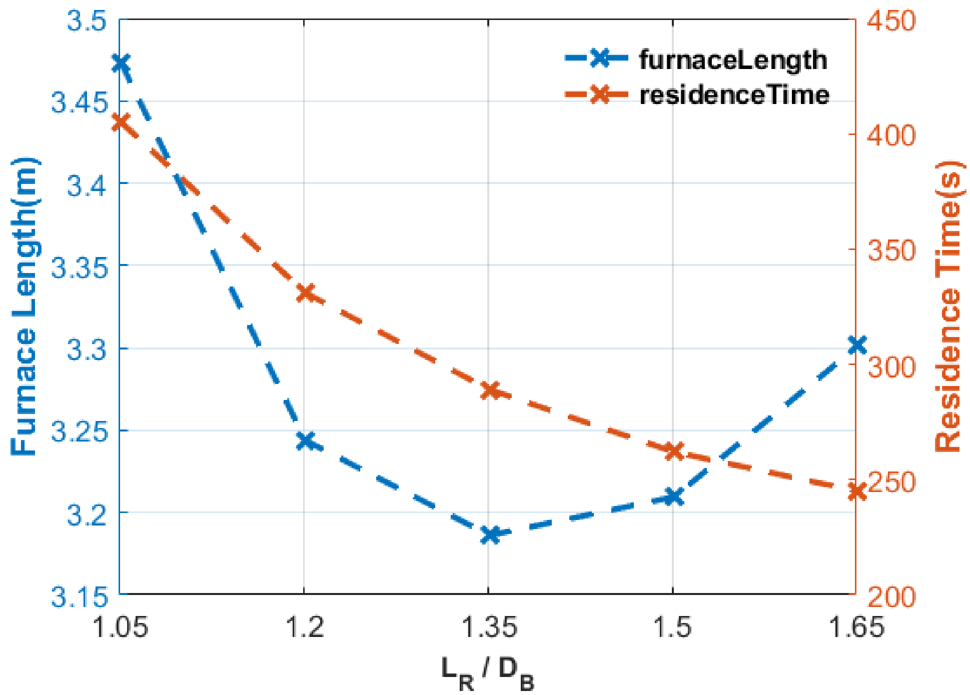

Figure 13: Optimal length of heating section

Figure 13 shows the variation in the residence time of the bottles and in the length of furnace with respect to the nondimensional spacing between the bottle rows shown in x-axis. The residence time decreases with the increase in the spacing between the bottle rows. This is due to the increase in the incoming radiative heat flux on the glass surface resulting from the rise in the view factor between the glass and the furnace walls. Consequent reduction in the shadowing effect results in a parabolic variance in the overall heating zone length. The dimensionless spacing of 1.05, with the conditon that there is almost no space between the rows of bottles, represents the longest length zone due to the shadowing effect. As the spacing is increased, the length of the heating zone reduced until the spacing reaches 1.35. This point expresses the most effective linear arrangement of the bottles in terms of heating for the considered bottle geometry. Opening the spacing between the rows more than this value results in an increase in the required heating zone length. As the spacing increases, the speed of the conveyor belt must be increased to keep the throughput the same. From the optimum point, the speed of conveyort belt becomes the dominant factor to determine the length of furnace.

4.5 Heating characteristic of bottles

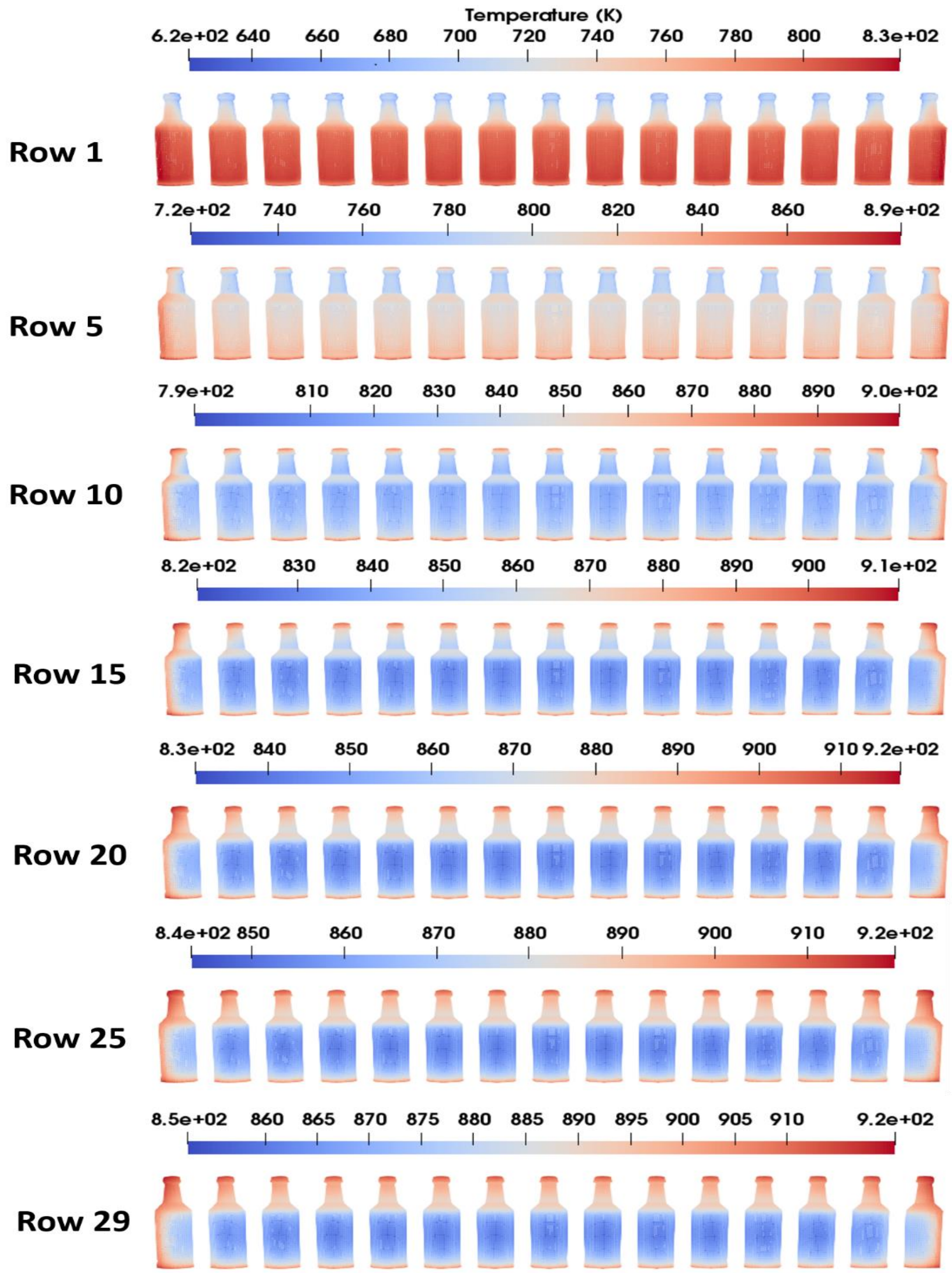

Figure 14: Surface temperatures of bottles at different rows during heating

The temperature distribution of the outer surface of the bottles is depicted in Figure 14 for different rows numbers. At the entrance to the furnace described in row 1, the bottles have common temperature distribution, except for the slighly lower temperature bottles at the edge and the neck of the bottles. During transport from molding machines to the furnace entrance, the surface temperature of interior bottles is maintained, but the surface of the side bottles and the upper region of the all bottles exposed to the environment loses more heat. This caused a temperature deviation across the height of bottles. In the topmost region of the bottles, mouth, has the lowest temperature around 670 K. Temperature on the neck is deviating around 720 K. At lower level, shoulder region is on 760 K. The largest region of the bottles, body has the highest temeperature as 820 K. Compared to all rows in the furnace, the maximum temperature is also observed in the first row, which is about 150 K. From this row, the bottles in the heating zone are gradually heated. However, the heating trend is not the same. The bottles on the outer edge of the rows heat up faster than the other, as expected. On the other hand, heating is unevenly on the edge bottles. The temperature of the side surface facing the side furnace wall increases quicker than the opposite side surface. This is because these bottles receive more radiative heat flux from the furnace wall due to their special position in the row. Common in all bottles, the neck and base of the bottles also heat up more strongly than the other regions whereas the body still taken a time. The reason for that is the view factor on the neck is relatively higher due to the higher lateral gap between the bottle neck, and the bases are received heat fluxes from the bottom of the furnace without any attenuation. On the other hand, the body of the bottles received the least radiative heat fluxes. This is due to the shadowing effect of other bottles. Shading effects are managed throughout the furnace, even at the furnace exit, row 29, the temperature differences drop to about 65 K.

The internal temperature distribution of the bottles inside the furnace is shown in Figure 15. The temperature distribution withing bottles is similar to their surface temperature distribution. The bottles located next to the furnace walls are found to be heated the most, and they are subject of unevenly lateral heating. Moreover, the bottles in the same row throughout the furnace, the upper region and the base temperature rise faster than the body. At the furnace entrance, row 1, the temperture of the regions of the edge bottles on the side of furnace wall is in harmony with the regions on the opposite sides. From the 1st row, the temperature difference between the opposite side starts to develop. This is because the bottles are opaque and do not allow the heat flows emanating from the side wall to pass through the bottle walls. The radiative heating between inner walls of the bottles is also considered in this model. However, it seems that the radiative heating between the internal walls can not completely compensate for the nonuniform radiative heat flux distribution on the outer walls of those bottles at the outer edge of the rows. In all bottles, lateral temperature distribution from outer walls to the interior is continuous since the only option of heat dissipation within the bottles by conduction [1]. Also, the low conduction resistance due to the relatively thin wall of the bottle prevents high temperature gradients from forming inside the bottles.

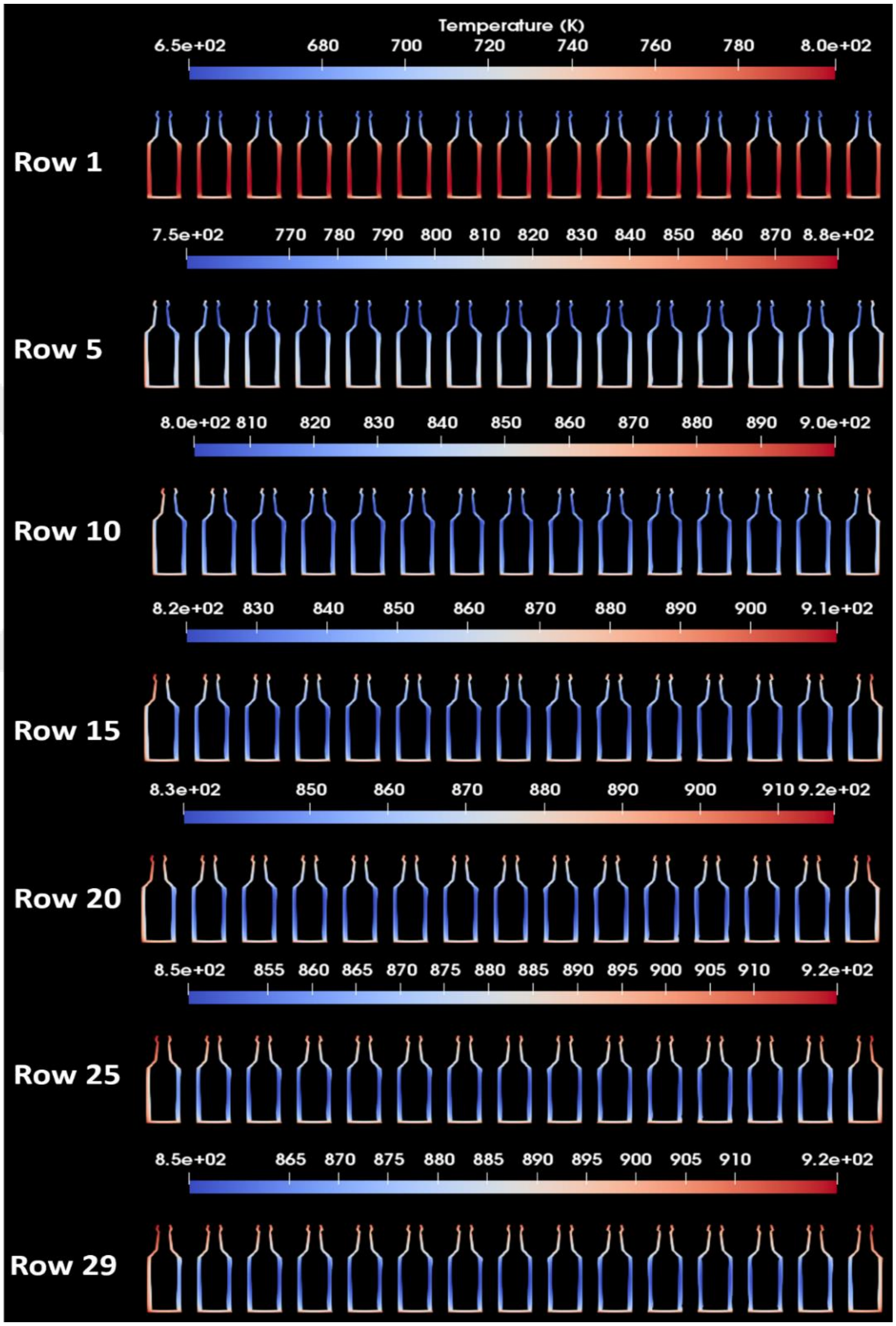

Figure 15: Internal temperature of bottles during heating

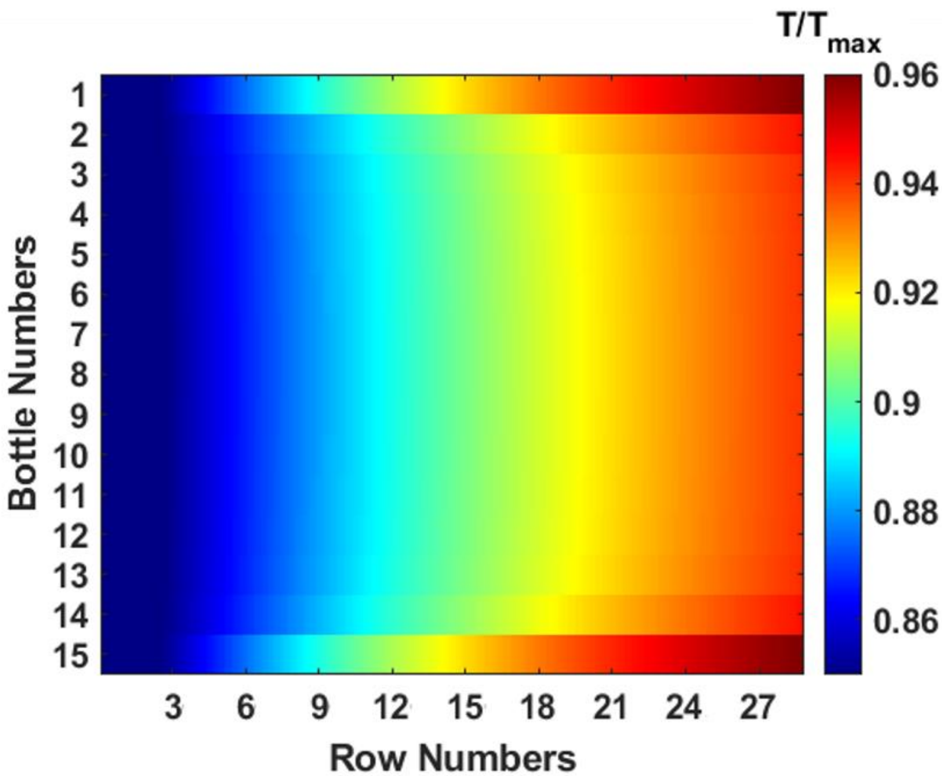

Figure 16: Volume average temperature of rows during operation

Figure 16 covers the volume average temperature of each bottle inside the heating zone of the furnace. All bottles have same volume average temperature at the beginning, yet the bottles on the edges are slightly lower. Bottles gradually heat up with time through the furnace. Most heated bottles are on the edge of a row as discussed before. There is a major temperature difference of about 14K between the edge bottles and its neighbor at the same row. This inditaces that emitted radiative heat fluxes from the side of the furnace wall is heavily blocked by edge bottles. There is about 3K difference between the average temperatures of the 2nd and 3rd bottles. However, from that point on towards the center of the row no considerable average temperature differences between the bottles were observed.

4.6 Computational Investigations of solver

In this section, performance of hybird CPU-GPU solver is examined with four scenarios each consisting of 5,10,15 and 20 bottles per row. In all the simulations seven rows of bottles are included. Moreover, the simulations are runned with different number of rays. The heat conduction calculations are carried on a single core of Intel Core i7 8700k CPU. In-house developed radiation model is performed with intermediate level gaming graphic processor unit NVIDIA GeForce GTX 1050Ti. Table 5 shows the measured computational time of the second order radiation model according to number of rays and number of surface mesh size. As shown, the number of the bottles in the domain has a weak influence on the computational time thanks to the AABB type accelerating structure used in the implementation. On the other hand, the number of rays used in the calculation has a first order effect on the computational time. Results show that in all the simulations the computational time is almost nearly proportional to the number of rays used in the simulations.

Table 5: Computational cost of second order radiation model

Emitted number of rays per iteration	35Bottles (1,024,800 primitives)	70Bottles (2,049,600 primitives)	105Bottles (3,074,400 primitives)	140Bottles (4,099,200 primitives)
12m	0.2869	0.3232	0.3618	0.4475
80m	1.8243	2.1339	2.2898	2.3203
160m	3.5815	3.9981	4.3666	4.5017
490m	10.708	12.1958	12.9858	13.1658
640m	14.5305	15.3867	16.6338	17.0805
810m	17.9975	19.1606	20.9251	21.5432
1b	22.6645	23.6241	25.3332	26.2356
2b	43.6929	47.4906	51.0016	51.8694
3b	63.6552	71.0006	76.0014	77.2746
4b	85.2870	93.1125	100.8018	102.757

Table 6: Computational time for heat conduction solving

Computationa time per iteration(s)	35Bottles (2,716,560 cells)	70Bottles (5,433,120 cells)	105Bottles (8,149,680 cells)	140Bottles (10,866,240 cells)
Heat conduction solver	1.2362	2.6564	4.0271	6.3835

Table 6 shows the computational time for the heat conduction equation solving by OpenFOAM. Results indicate that computational time is increased more than by factor of 2 while number of bottles are included in the simulation.

Table 7: Computational time for data transfer between CPU and GPU

Computational time per iteration(s)	35Bottles (1,024,800 primitives)	70Bottles (2,049,600 primitives)	105Bottles (3,074,400 primitives)	140Bottles (4,099,200 primitives)
Data Transfer	0.0071	0.0110	0.0161	0.0209

Table 6 indicates that data transfer between the GPU and CPU where the radiation and conduction calculations are conducted respectively. In each iteration, surface temperatures are sent from CPU to GPU and their correspoding heat fluxes are sent from GPU to CPU. Size of temperature and size of heat flux datas are equall to number of primitives on the surface. Computational time of data transfer is increased around by factor of 1.5 while the primitive numbers is increased. However, compared to the cost of the radiation and conduction calculations they are negligible.

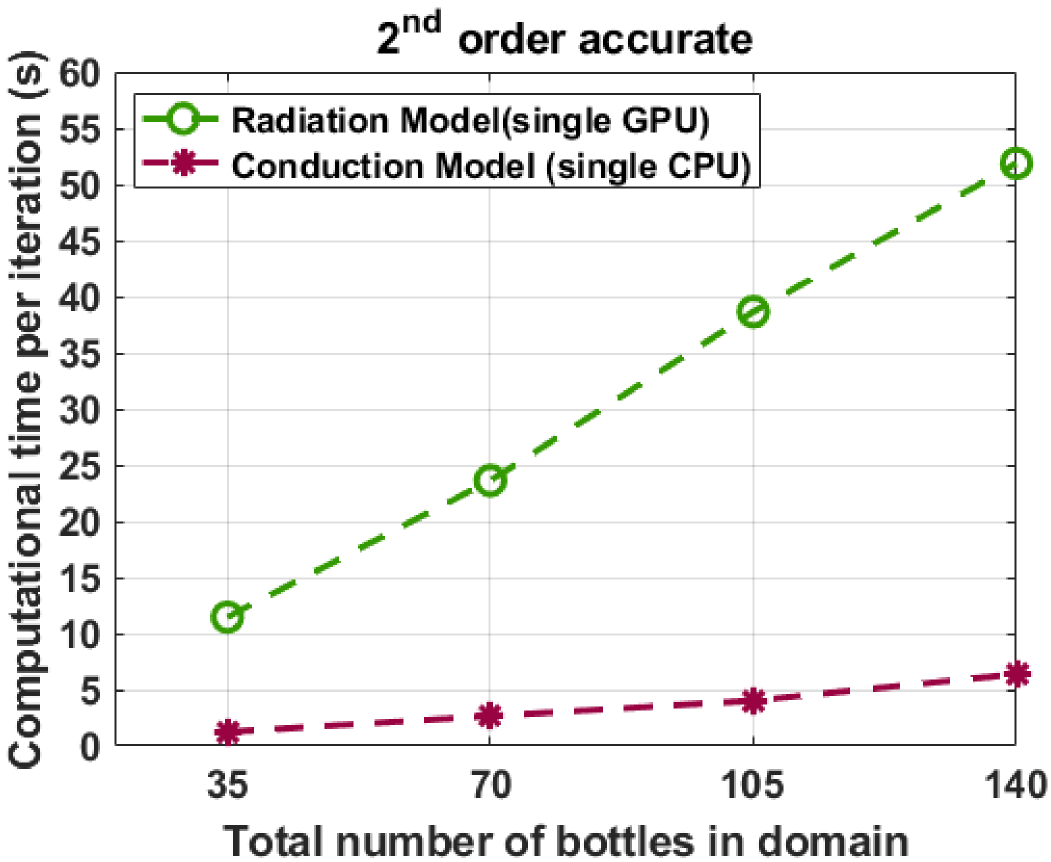

Figure 17*:* Computational time per time step for the radiation model (GPU) and conduction model (CPU) for the simulations with 5, 10 15 and 20 bottles in a row.

Finally, the computational cost of the hybrid solver is evaluated with respect to the number of bottles within the heating section of the furnace. For a fair comparison the number of rows is fixed to 7 and the number of rays used per bottles is also fixed to 355 rays per surface face. It results in a belower than standard deviation of 5% of the mean radiative heat flux. Figure 17 shows that. Required computational time for the simulations are nearly linearly increased while the number of meshes increased. In all cases, the computational cost of the simulations are quitely dominated by the 2^{nd} order accurate radiation model. The amount of %90 of the total computational time belongs to radiation calculations and only 10% is by conduction calculations. The total calculation time (radiation + conduction) per iteration takes about 43 s per for the scenario with 105 bottles in the furnace. On the other hand, computational time of first order accurate model is directly 30% less than second order accurate model which is about 30s, since it is deduced from first order accuracate model with consecutively executed three computations. Previously mentioned about error rates of first order model at Δt =2 s and second order model at Δt =5 s are nearly equal and in strong accuracy which is below 1K. Under those time step condition, second order accurate model yields x1.75 times speed up against the first order accurate model. Required computational time per iteration becomes 8.6 s and 15 s for second order accurate model and first order accurate model, respectively.

CHAPTER V

CONCLUSION

Transient radiative heating of 3D moving bottles inside heating section of the continuos annealing furnace is investigated. Problem inside the heating section of electrally heated furnace is considered combined conduction-radiation problem. Conduction and radiation calculations are seperately conducted by hybrid CPU-GPU solver. On the GPU side of the solver, an in-house developed Backward Monte Carlo Ray Tracing method is introduced to solve radiative heat fluxes on the surface of the moving bottles. Radiative heat fluxes are calculated between bottles at the same row, between bottles at the neighbour row and between bottles and furnace walls. Boundary condition of surfaces inside furnace is considered diffuse emitter and black. Due to black assumption, heat fluxes on the surface of bottles are overestimated about 25%. On the CPU side, the heat conduction equation is solved by imposing radiative heat fluxes as boundary condition. Conduction equation is discretized with 2^{nd} order accurate central method in space and with 1^{st} order accurate Backward Euler method in time. In the computational furnace model, rather than considering the heating section fully loaded with 29 bottle rows, 7 bottle rows are propounded to represent fully loaded furnace condition. Among 7 bottle rows only the 4^{th} row is designated to represent the temperature distribution of bottles in the furnace. Nevertheless, the temperature of the bottles inside other rows is also solved since they act boundary condition of the bottles for the row 4. Due to the stochastic nature of Monte Carlo method, the accuracy of the radiation model is increased while the number of rays used in calculations is increased. In this regard, 355 rays per surface face are used in the radiation calculations results in the standard deviation of about 3.5% to the mean of heat flux level with reasonable computational effort. The second order accurate radiation model showed less biased results compared to first order accurate method. The Optimal design point of the furnace is actualized by the distance between rows are founded as 0.11m (L_R/D_B = 1.35). 3D heating characteristics of 29 bottle rows, 435 bottles, are succesfully analyzed. It has been found that upper region and the base are the most heated sections of the bottles, and the most heated bottles are the edge bottles. There is a significant temperature decrease from edge bottles to their neighbour bottle which is about 14 K. At the exit of the furnace temperature difference within the same row observed around 150 K. Main conclusions about the research as follows:

- By only considering 7 bottle rows instead of 29 bottle rows inside the heating section, the total computation time of numerical simulations are decreased by more than 4 times with error rate below than 1%.
- Since the conduction calculations are repeatedly performed on a singel bottle rows mesh, the memory requirement of the simulation is decreased by 29 times.
- With the Backward Monte Carlo Ray Tracing method efficiency of radiation calculations are increased. Moreover, row by row radiation calculations is enabled to

increase the number of emission of rays in a single iteration by 7 times, which result in higher accuracy.

- Second order accurate model showed significantly better results than first order accurate model.
- Second order accurate model gained x1.75 speed-up in the simulations with 1K error temperature error rate.
- Optimal design point of furnace is achieved by the spacing of bottle rows. In this regard, residence time of bottles are decreased about 150 seconds and the length of furnace is shortened about 8.6% compared to almost no spacing between bottle rows.
- It has been found that radiative calculations are heavily dominant over heat conduction calculations. 91% of the total computational time constituted by radiation calculations.

5.1 Future Works

We are suggesting to further development and enrichment the study.

- Convective heat transfer will be taken into account with a separate CFD model or a mutual feature of current solver. It is on the progress.
- Experimental setup of electirically heated furnace will be established and experiments will be conducted. It is on the progress.
- Higher order accuracy in time discretization and space will be implemented to solver.

- Wavelength dependency of glassware will be implemented.
- More efficient and robust computational model is on the progress.

BIBLIOGRAPHY

[1] R. GARDON, “A Review of Radiant Heat Transfer in Glass,” *J. Am. Ceram. Soc.*, vol. 44, no. 7, pp. 305–312, 1961, doi: 10.1111/j.1151-2916.1961.tb15914.x.

[2] S. Silvestri and R. Pecnik, “A fast GPU Monte Carlo radiative heat transfer implementation for coupling with direct numerical simulation,” *J. Comput. Phys. X*, vol. 3, 2019, doi: 10.1016/j.jcpx.2019.100032.

[3] M. Overby, P. Willemsen, B. N. Bailey, S. Halverson, and E. R. Pardyjak, “A rapid and scalable radiation transfer model for complex urban domains,” *Urban Clim.*, vol. 15, pp. 25–44, 2016, doi: 10.1016/j.uclim.2015.11.004.

[4] A. Humphrey, T. Harman, M. Berzins, and P. Smith, “A scalable algorithm for radiative heat transfer using reverse monte carlo ray tracing,” *Lect. Notes Comput. Sci. (including Subser. Lect. Notes Artif. Intell. Lect. Notes Bioinformatics)*, vol. 9137 LNCS, pp. 212–230, 2015, doi: 10.1007/978-3-319-20119-1_16.

[5] H. Takizawa, N. Yamada, S. Sakai, and H. Kobayashi, “Radiative heat transfer simulation using programmable graphics hardware,” *Proc. - 5th IEEE/ACIS Int. Conf. Comput. Info. Sci., ICIS 2006. conjunction with 1st IEEE/ACIS, Int. Work. Component-Based Softw. Eng., Softw. Arch. Reuse, COMSAR 2006*, vol. 2006, pp. 29–37, 2006, doi: 10.1109/ICIS-COMSAR.2006.70.

[6] A. Humphrey, D. Sunderland, T. Harman, and M. Berzins, “Radiative heat transfer calculation on 16384 GPUs using a reverse Monte Carlo ray tracing approach with adaptive mesh refinement,” *Proc. - 2016 IEEE 30th Int. Parallel Distrib. Process. Symp. IPDPS 2016*, pp. 1222–1231, 2016, doi: 10.1109/IPDPSW.2016.93.

[7] E. Alerstam, T. Svensson, and S. Andersson-Engels, “Parallel computing with graphics processing units for high-speed Monte Carlo simulation of photon migration,” *J. Biomed. Opt.*, vol. 13, no. 6, p. 060504, 2008, doi: 10.1117/1.3041496.

[8] F. P. Siddiqui, K. Menekşedağ, A. M. Basol, and M. P. Mengüç, “Combined Radiation and Conduction Heat Transfer Solver on Hybrid Cpu-Gpu Architectures,” no. December, 2018.

[9] M. Gu, G. Chen, X. Liu, C. Wu, and H. Chu, “Numerical simulation of slab heating process in a regenerative walking beam reheating furnace,” *Int. J. Heat Mass Transf.*, vol. 76, pp. 405–410, 2014, doi: 10.1016/j.ijheatmasstransfer.2014.04.061.

[10] S. H. Han, D. Chang, and C. Y. Kim, "A numerical analysis of slab heating characteristics in a walking beam type reheating furnace," *Int. J. Heat Mass Transf.*, vol. 53, no. 19–20, pp. 3855–3861, 2010, doi: 10.1016/j.ijheatmasstransfer.2010.05.002.

[11] R. Prieler, B. Mayr, M. Demuth, B. Holleis, and C. Hochenauer, "Numerical analysis of the transient heating of steel billets and the combustion process under air-fired and oxygen enriched conditions," *Appl. Therm. Eng.*, vol. 103, pp. 252–263, 2016, doi: 10.1016/j.applthermaleng.2016.04.091.

[12] S. H. Han and D. Chang, "Optimum residence time analysis for a walking beam type reheating furnace," *Int. J. Heat Mass Transf.*, vol. 55, no. 15–16, pp. 4079–4087, 2012, doi: 10.1016/j.ijheatmasstransfer.2012.03.049.

[13] J. M. Casal, J. Porteiro, J. L. Míguez, and A. Vázquez, "New methodology for CFD three-dimensional simulation of a walking beam type reheating furnace in steady state," *Appl. Therm. Eng.*, vol. 86, pp. 69–80, 2015, doi: 10.1016/j.applthermaleng.2015.04.020.

[14] S. H. Han, S. W. Baek, and M. Y. Kim, "Transient radiative heating characteristics of slabs in a walking beam type reheating furnace," *Int. J. Heat Mass Transf.*, vol. 52, no. 3–4, pp. 1005–1011, 2009, doi: 10.1016/j.ijheatmasstransfer.2008.07.030.

[15] M. Y. Kim, "A heat transfer model for the analysis of transient heating of the slab in a direct-fired walking beam type reheating furnace," *Int. J. Heat Mass Transf.*, vol. 50, no. 19–20, pp. 3740–3748, 2007, doi: 10.1016/j.ijheatmasstransfer.2007.02.023.

[16] A. Emadi, A. Saboonchi, M. Taheri, and S. Hassanpour, "Heating characteristics of billet in a walking hearth type reheating furnace," *Appl. Therm. Eng.*, vol. 63, no. 1, pp. 396–405, 2014, doi: 10.1016/j.applthermaleng.2013.11.003.

[17] A. Emadi, A. Saboonchi, M. Taheri, and S. Hassanpour, "Heating characteristics of billet in a walking hearth type reheating furnace," *Appl. Therm. Eng.*, vol. 63, no. 1, pp. 396–405, 2014, doi: 10.1016/j.applthermaleng.2013.11.003.

[18] J. Harish and P. Dutta, "Heat transfer analysis of pusher type reheat furnace," *Ironmak. Steelmak.*, vol. 32, no. 2, pp. 151–158, 2005, doi: 10.1179/174328105X23923.

[19] R. Dou *et al.*, "Numerical model and optimization strategy for the annealing process of 3D coil cores," *Appl. Therm. Eng.*, vol. 178, no. January, p. 115517, 2020, doi: 10.1016/j.applthermaleng.2020.115517.

[20] N. Depree *et al.*, "Development and validation of models for annealing furnace control from heat transfer fundamentals," *Comput. Chem. Eng.*, vol. 34, no. 11, pp. 1849–1853, 2010, doi: 10.1016/j.compchemeng.2010.01.012.

[21] L. Jadachowski, A. Steinboeck, and A. Kugi, “Heat transfer with specular reflections in an experimental annealing device,” *IFAC-PapersOnLine*, vol. 28, no. 1, pp. 494–499, 2015, doi: 10.1016/j.ifacol.2015.05.069.

[22] L. Jadachowski, A. Steinboeck, and A. Kugi, “Two-dimensional thermal modelling with specular reflections in an experimental annealing furnace,” *Math. Comput. Model. Dyn. Syst.*, vol. 23, no. 1, pp. 23–39, 2017, doi: 10.1080/13873954.2016.1237969.

[23] L. Jadachowski, A. Steinboeck, and A. Kugi, “Feedforward Control of the Temperature Field in an Experimental Annealing Furnace,” *IFAC-PapersOnLine*, vol. 50, no. 1, pp. 13790–13795, 2017, doi: 10.1016/j.ifacol.2017.08.2068.

[24] L. Jadachowski, A. Steinboeck, and A. Kugi, “Model Averaging and Feedforward Temperature Control in an Oscillating Annealing Furnace,” *IFAC-PapersOnLine*, vol. 51, no. 21, pp. 163–168, 2018, doi: 10.1016/j.ifacol.2018.09.410.

[25] F. Maislinger, M. Niederer, A. Steinboeck, S. Strommer, and A. Kugi, “A Mathematical Model of a Horizontal Direct-Fired Strip Annealing Furnace,” *IFAC-PapersOnLine*, vol. 49, no. 20, pp. 202–207, 2016, doi: 10.1016/j.ifacol.2016.10.121.

[26] L. Pyta, A. Deutschmann, F. Rötzer, D. Abel, and A. Kugi, “Reduced-order modeling of a radiative heating process with movable radiators,” *IFAC-PapersOnLine*, vol. 52, no. 16, pp. 346–351, 2019, doi: 10.1016/j.ifacol.2019.11.804.

[27] A. Jaklič, T. Kolenko, and B. Zupančič, “The influence of the space between the billets on the productivity of a continuous walking-beam furnace,” *Appl. Therm. Eng.*, vol. 25, no. 5–6, pp. 783–795, 2005, doi: 10.1016/j.applthermaleng.2004.07.012.

[28] O. M. H. Fatla, A. Valera-Medina, F. Robinson, M. Cichuta, and N. Beynon, “Development of convection in high temperature coil annealing furnaces using rotating cylinder technique,” *Appl. Therm. Eng.*, vol. 129, pp. 1392–1402, 2018, doi: 10.1016/j.applthermaleng.2017.10.136.

[29] S. H. Han, D. Chang, and C. Huh, “Efficiency analysis of radiative slab heating in a walking-beam-type reheating furnace,” *Energy*, vol. 36, no. 2, pp. 1265–1272, 2011, doi: 10.1016/j.energy.2010.11.018.

[30] S. H. Han, Y. S. Lee, J. R. Cho, and K. H. Lee, “Efficiency analysis of air-fuel and oxy-fuel combustion in a reheating furnace,” *Int. J. Heat Mass Transf.*, vol. 121, pp. 1364–1370, 2018, doi: 10.1016/j.ijheatmasstransfer.2017.12.110.

[31] A. M. García and A. A. Amell, “A numerical analysis of the effect of heat recovery burners on the heat transfer and billet heating characteristics in a walking-beam type reheating furnace,” *Int. J. Heat Mass Transf.*, vol. 127, pp. 1208–1222, 2018, doi:

10.1016/j.ijheatmasstransfer.2018.07.121.

[32] N. Bayat, S. Mehraban, and S. M. H. Sarvari, “Inverse boundary design of a radiant furnace with diffuse-spectral design surface,” *Int. Commun. Heat Mass Transf.*, vol. 37, no. 1, pp. 103–110, 2010, doi: 10.1016/j.icheatmasstransfer.2009.07.005.

[33] S. M. H. Sarvari, S. H. Mansouri, and J. R. Howell, “Inverse boundary design radiation problem in absorbing-emitting media with irregular geometry,” *Numer. Heat Transf. Part A Appl.*, vol. 43, no. 6, pp. 565–584, 2003, doi: 10.1080/10407780307350.

[34] S. H. Mansouri, “Inverse Boundary Design Conduction-Radiation Problem In Irregular Two-Dimensional Domains,” *Numer. Heat Transf. Part B Fundam.*, vol. 44, no. 3, pp. 209–224, 2003, doi: 10.1080/713836377.

[35] H. Amiri, S. H. Mansouri, A. Safavinejad, and P. J. Coelho, “The optimal number and location of discrete radiant heaters in enclosures with the participating media using the micro genetic algorithm,” *Numer. Heat Transf. Part A Appl.*, vol. 60, no. 5, pp. 461–483, 2011, doi: 10.1080/10407782.2011.600597.

[36] F. Erchiqui, “Application of genetic and simulated annealing algorithms for optimization of infrared heating stage in thermoforming process,” *Appl. Therm. Eng.*, vol. 128, pp. 1263–1272, 2018, doi: 10.1016/j.applthermaleng.2017.09.102.

[37] S. M. Hosseini Sarvari, S.H. Mansouri and J. R. Howell, "INVERSE DESIGN OF THREE-DIMENSIONAL ENCLOSURES WITH TRANSPARENT AND ABSORBING-EMITTING MEDIA USING AN OPTIMIZATION TECHNIQUE," *Int. Comm. Heat Mass Transfer*, Vol. 30, No. 2,pp.149-162, 2003

[38] R. P. Chopade, S. C. Mishra, P. Mahanta, and S. Maruyama, “Effects of locations of a 3-D design object in a 3-D radiant furnace for prescribed uniform thermal conditions,” *Appl. Therm. Eng.*, vol. 31, no. 16, pp. 3262–3274, 2011, doi: 10.1016/j.applthermaleng.2011.05.047.

[39] A. SAFAVINEJAD, S. MARUYAMA, S. H. MANSOURI, and A. SAKURAI, “Optimal Boundary Design of Radiant Enclosures Using Micro-Genetic Algorithm (Effects of Refractory Properties and Aspect Ratio of Enclosure on Heaters Setting),” *J. Therm. Sci. Technol.*, vol. 3, no. 2, pp. 179–194, 2008, doi: 10.1299/jtst.3.179.

[40] R. P. Chopade, S. C. Mishra, P. Mahanta, and S. Maruyama, “On configuration of load in radiant furnace for uniform thermal conditions,” *Heat Transf. Eng.*, vol. 35, no. 1, pp. 94–109, 2014, doi: 10.1080/01457632.2013.810461.

[41] E. Yıldız, A. M. Başol, and M. P. Mengüç, “Segregated modeling of continuous heat treatment furnaces,” *J. Quant. Spectrosc. Radiat. Transf.*, vol. 249, pp. 1–10, 2020, doi: 10.1016/j.jqsrt.2020.106993.

[42] https://www.openfoam.com/documentation/guides/latest/api/index.html

[43] https://www.openfoam.com/documentation/guides/latest/api/index.html

[44] Howell, J.R., Menguc, M.P., & Siegel, R. (2015). Thermal Radiation Heat Transfer (6th ed.). CRC Press.

[45] S. G. Parker *et al.*, “OptiX: A general purpose ray tracing engine,” *ACM SIGGRAPH 2010 Pap. SIGGRAPH 2010*, 2010, doi: 10.1145/1778765.1778803.

[46] T. L. Kay and J. T. Kajiya, “Ray tracing complex scenes,” *Proc. 13th Annu. Conf. Comput. Graph. Interact. Tech. SIGGRAPH 1986*, vol. 20, no. 4, pp. 269–278, 1986, doi: 10.1145/15922.15916.

[47] “A catalog of radiation configuration factors." http://www.thermalradiation.net/indexCat.html.

[48] Crawford, Martin, 1972, "Configuration factor between two unequal, parallel, coaxial squares," paper no. *ASME* 72-WA/HT-16

[49] http://www.thermalradiation.net/calc/sectionc/C-12.html